

Accepted Manuscript

Effect of substituent dependent molecular structure on anti-corrosive behavior of one-pot multicomponent synthesized pyrimido [2,1-B] benzothiazoles: Computer modelling supported experimental studies



Chandrabhan Verma, M.A. Quraishi, I.B. Obot, Eno E. Ebenso

PII: S0167-7322(19)31786-6
DOI: <https://doi.org/10.1016/j.molliq.2019.110972>
Article Number: 110972
Reference: MOLLIQ 110972
To appear in: *Journal of Molecular Liquids*
Received date: 28 March 2019
Revised date: 6 May 2019
Accepted date: 13 May 2019

Please cite this article as: C. Verma, M.A. Quraishi, I.B. Obot, et al., Effect of substituent dependent molecular structure on anti-corrosive behavior of one-pot multicomponent synthesized pyrimido [2,1-B] benzothiazoles: Computer modelling supported experimental studies, Journal of Molecular Liquids, <https://doi.org/10.1016/j.molliq.2019.110972>

This is a PDF file of an unedited manuscript that has been accepted for publication. As a service to our customers we are providing this early version of the manuscript. The manuscript will undergo copyediting, typesetting, and review of the resulting proof before it is published in its final form. Please note that during the production process errors may be discovered which could affect the content, and all legal disclaimers that apply to the journal pertain.

Effect of Substituent Dependent Molecular Structure on Anti-Corrosive Behavior of One-Pot Multicomponent Synthesized Pyrimido [2,1-B] Benzothiazoles: Computer Modeling Supported Experimental Studies

Chandrabhan Verma^{a,b*}, M. A. Quraishi^b, I. B. Obot^b and Eno E. Ebenso^{a*}

^aDepartment of Chemistry, School of Mathematical & Physical Sciences, and Material Science Innovation & Modelling (MaSIM) Research Focus Area, Faculty of Agriculture, Science and Technology, North-West University (Mafikeng Campus), Private Bag X2046, Mmabatho 2735, South Africa

^bCenter of Research Excellence in Corrosion, Research Institute, King Fahd University of Petroleum & Minerals, Dhahran 31261, Saudi Arabia

Corresponding Author's emails:

chandrabhan.rs.apc@itbhu.ac.in (CV), eno.ebenso@gmail.com (EEE)

Abstract

The present study is designed to demonstrate the substituent dependent molecular structures on inhibition property of four heterocyclic compounds containing nitrogen, sulfur and oxygen atoms for mild steel corrosion in 1M HCl. Their inhibition effect was measured using weight loss, open circuit potential (OCP), potentiodynamic polarization (PDP) and electrochemical impedance spectroscopy (EIS), scanning electron microscopy (SEM) and atomic force microscopy (AFM) and computational methods. Outputs of the experimental and computation studies showed that their inhibition efficiencies followed the order: PBT-IV (–OCH₃+ –OH) > PBT-III (–OH) > PBT-II (–CH₃) > PBT-I (–H). Among tested compounds, PBT-IV acted as best corrosion inhibitor and showed highest inhibition efficiency of 94.88% at 42.8×10^{–5} M concentration. Presence of PBTs in the acidic medium causes increase in the value of R_{ct} and decrease in the value of current density (i_{corr}). DFT results showed that the presence of electron releasing substituents (–OCH₃, –OH and –CH₃) enhance the electron density on the frontier molecular orbitals responsible for the metal surface-inhibitors interactions. The molecular structures of the investigated compounds possess the ability of high electron donation (high E_{HOMO}) as well as acceptance (low E_{LUMO}). Molecular alignment of inhibitors on the metallic surface was determined MD simulations study which showed that they aligned horizontally (flatly) on the metallic surface that offers the high protection ability. Polarization study showed that mainly they acted as a cathodic type of inhibitors. The results of computational and experimental studies were consistent.

Keywords: Structural effect, electronic factors, Corrosion inhibitors, Computational simulations,

1. Introduction

Degradation of the metallic materials (pure metals and alloys) by the interactions with components of surrounding environment is known as corrosion [1]. Corrosion is an extremely dangerous process during the industrial cleaning of the metallic ores. As per the study of NACE (National Association of Corrosion Engineers) United State losses around US \$ 276 billion and US \$ 2.2 trillion due to corrosion in the years 1998 and 2011, respectively. A recent estimation of NACE shows that current economic loss of corrosion has been increased up to US \$ 2.2 trillion that equates around 3.4% of the gross domestic product (GDP) [2-4]. In order to avoid the excessive corrosive loss of metallic materials some external additives (known as corrosion inhibitors) are required to be added in the cleaning solutions [5, 6]. Application of the synthetic organic inhibitors is one of the best methods because of their high effectiveness at relatively low concentration [7, 8]. The organic inhibitors contain several polar functional groups and conjugated non-bonding and π electrons which can behave as adsorption centers during metal-inhibitor bonding. Along with non-bonding and π electrons of the multiple bonds, molecular structural properties play significant role while determining the effectiveness of the organic corrosion inhibitors [9-11].

Molecular structural effect

There are several salient molecular structural features required for a molecule to be acted as efficient corrosion inhibitors. Planarity of the organic corrosion inhibitors plays a significant role toward metallic corrosion inhibition as a planer molecule adsorbs by flat or horizontal alignment and thereby covers larger metallic surface and protective largely from corrosion as compared to the corrosion inhibitors having non-planer or vertical alignment [12, 13]. A more soluble corrosion inhibitor acts as better corrosion as compared to the relatively less corrosion inhibitor [14, 15]. Generally, organic corrosion inhibitors are heterocyclic compounds containing polar functional groups such as $-\text{CH}_3$, $-\text{NMe}_2$, $-\text{NH}_2$, $-\text{NO}_2$, $-\text{OH}$, $-\text{OMe}$, $-\text{SO}_3\text{H}$, $-\text{CONH}_2$, $-\text{COOC}_2\text{H}_5$ and $-\text{COOH}$ which can enhance the solubility of the inhibitor molecules in the polar electrolytic media and also behave as adsorption centers [16, 17]. Hammett equation can be used most appropriately in order to explain the effect of substituents. The Hammett equation and its simplified forms for substituent effect are presented bellows [9-11]:

$$\log \frac{K_R}{K_H} = \rho\sigma \quad (1)$$

$$\log \frac{1-\eta\%_R}{1-\eta\%_H} = \rho\sigma \quad (2)$$

$$\log \frac{\eta\%_R}{\eta\%_H} = \rho\sigma - \log \frac{\theta_R}{\theta_H} \quad (3)$$

whereas, σ is known as the Hammett constant and basically related to the whole electronic effect of the substituent, ρ is a reaction parameter which gives information about the degree of metal-inhibitor interactions. The equilibrium constant values for inhibitors with and without substituents are presented by K_R and K_H , respectively. The $\eta\%_H$ and $\eta\%_R$ are the inhibition efficiencies of the inhibitor without and with substituent, respectively. And, θ_R and θ_H are the surface coverage values by the inhibitor molecule with and without substituent, respectively. From Hammett equations it is observable that nature of substituents exert significant effect on the corrosion inhibition efficiency of the organic inhibitors. In present study, four heterocyclic compounds were synthesized using the multicomponent reactions (MCRs) which is associated with several salient features such as high atom economy, high selectivity, ease to perform, lower number of purification and workups steps, high automation, shorter reaction time, high yield, minimum waste generation and high synthetic efficiency etc. which satisfy the need of green chemistry essentially required because of the increasing ecological awareness and strict environmental regulations [18-20]. More so, carbohydrate based catalysts such as chitosan are regarded as biodegradable, efficient, reusable, inexpensive, non-toxic and biodegradable that are essential requirement for a compound to be treated as “green chemicals” or “green catalyst” [21-23]. The synthesized heterocyclic compounds are investigated as corrosion inhibitors for mild steel in 1M HCl using experimental and computational approaches.

2. Experimentals

The chemicals employed in the synthesis were purchased from sigma Aldrich. The molecular weight of chitosan was 190,000 Da. Similar to the previously described method, investigated inhibitors (PBTs) were synthesized using one step multicomponent reaction of benzaldehyde derivatives (10 mmol), ethyl acetoacetate (10 mmol; 1.301g) and 2-aminobenzothiazole (10 mmol; 1.502g) in the presence of 0.16 g chitosan dissolved in 2% aqueous solution of acetic acid (20 ml) at $65 \pm 2^\circ\text{C}$ (Fig. 1) [23]. According to the reported reaction optimum time, reaction

mixtures were allowed to stirred and refluxed for 100 minutes and progress of the reactions were measured by thin layer chromatography (TLC) method. Products of desired purity were filtered out after the completion of the reactions. Their characterization results and data are presented in Table 1.

The inhibition effect of PBTs on mild steel acidic corrosion in 1M HCl was investigated using weight loss, surface and electrochemical methods. Composition in (weight percentage) of the mild steel specimens for all experiments was Mn (0.192%), Al (0.023%), Si (0.026%), Cr (0.050%), P (0.012%), C (0.076) and balanced with Fe. The area of mild steel specimens to be exposed in corrosive solution were abraded from SiC emery papers (600-1200 mesh size), washed and degreased with distilled water and acetone, respectively. The specimens after their cleaning and drying were stored in desiccators until they were used in the experiments. Electrolytic medium of 1M HCl was prepared by the dilution of the analytical grade HCl (37%) purchased from Merck Pvt. Ltd. Weight loss measurements were carried out similar to our previous reported papers [24, 25]. Accurately weighted mild steel specimens having dimension $0.025\text{ cm} \times 2.0\text{ cm} \times 2.5\text{ cm}$ were allowed to corrode in 100 ml unstirred solution of testing medium in the absence and presence of various concentrations of PBTs. After 3 hrs immersion time the specimens were taken out and weighted precisely again. The difference between initial and final weight of the specimens were served as basis for the determination of inhibition efficiencies of the PBTs at their several tested concentrations as per the following relationship [24, 25]:

$$\eta\% = \frac{w_0 - w_i}{w_0} \times 100 \quad (4)$$

where, w_0 and w_i are the weight loss of the specimens (in mg) in the absence and presence of PBTs, respectively. The electrochemical study was carried out using Gamry galvanostat/potentiostat having model G-300 instrument. The electrochemical data (EIS and PDP) were analyzed using Gamry Echem Analyst software installed in personal computer. The instrument comprises of three electrode assemblage in which saturated calomel, mild steel and platinum foil was used as reference, working and counter electrode, respectively. Before measuring the EIS and PDP behavior of PBTs on mild steel corrosion, the specimens were allowed to corrode freely with and without optimum concentration of the PBTs in order to measure the steady open circuit potential (OCP) for 20 minutes. The potential developed over metal/ electrolyte interfaces without applying any external potential is known as OCP.

Potentiodynamic polarization curves were measured by sweeping the electrode potential ± 250 mV away from the operational corrosion potential at the scan rate of 1 mV/ second. The polarization curves were extrapolated to derived potentiodynamic parameters including corrosion current density (i_{corr}). The inhibition efficiency of the PBTs was derived using following equation [24, 25]:

$$\eta\% = \frac{i_{corr}^0 - i_{corr}^i}{i_{corr}^0} \times 100 \quad (5)$$

where, i_{corr}^i and i_{corr}^0 are the current densities for mild steel corrosion taking place in the presence and absence of PBTs, respectively. At the OCP, EIS spectra were recorded using AC signal of 10 mV amplitude having the frequency range of 0.01 Hz to 100 kHz. Fitting of the Nyquist plots in the suitable equivalent circuit gives the value of charge transfer resistance. The inhibition efficiency was derived as follows [24, 25]:

$$\eta\% = \frac{R_{ct}^i - R_{ct}^0}{R_{ct}^i} \times 100 \quad (6)$$

Where, R_{ct}^i and R_{ct}^0 are the charge transfer resistance values for mild steel dissolution in acidic medium with and without PBTs, respectively.

Surface morphological analyses of the inhibited by PBTs and uninhibited metallic surfaces were carried out using atomic force microscopy (AFM) and scanning electron microscopy (SEM) analyses. NT-MDT multimode AFM (Russia) and Ziess Evo 50 XVP instruments were used for AFM and SEM analyses, respectively. The mild steel specimens were allowed to corrode for 3 hrs in the absence and presence of optimum concentration of PBTs. After that the specimens were taken out, washed and analyzed using SEM and AFM instruments. The sample scanning area for AFM analysis was $5\mu\text{m} \times 5\mu\text{m}$ whereas the SEM images were taken at 2000x magnification.

Besides the experimental methods, computational modeling using DFT and MD simulations were adopted to describe the molecular interactions of PBTs with metallic surface. The DFT study was carried out using B3LYP functional and several commonly used basis sets such as 3-21G, 6-31G and 6-311G. Gaussian 09 software was undertaken for all DFT calculations. In acidic solution there is strong possibility of heteroatoms protonation therefore Mulliken charge of each atoms of PBTs was determined. The heteroatoms that have most negative Mulliken

charge were selected as cites for protonation and DFT study was carried out accordingly. For neutral as well as protonated PBTs, DFT parameters were derived using following formula [24, 25]:

$$\Delta E = E_{LUMO} - E_{HOMO} \quad (7)$$

$$\chi = -\frac{1}{2}(E_{LUMO} + E_{HOMO}) \quad (8)$$

$$\Delta N = \frac{\chi_{Fe} - \chi_{PBTs}}{2(\eta_{Fe} + \eta_{PBTs})} \quad (9)$$

where, ΔE is represents the energy band gap between energy of lowest unoccupied molecular orbital and highest occupied molecular orbital. The χ_{Fe} and χ_{PBTs} are the electronegativities of iron (7.0 eV, Pearson's electronegativity scale) and PBTs, respectively. The η_{Fe} and η_{PBTs} are the hardness of bulk iron (0 eV) and PBTs, respectively.

The interaction between the investigated inhibitors and Fe (110) plane surface was carried out using Monte Carlo simulations. The adsorption locator code implemented in the Material Studio 8.0 software from Biovia-Accelrys Inc. USA was adopted in this simulation. The COMPASS force field was used for the simulation of all molecules and systems. The simulation of the corrosion inhibitor molecules designated as PBT I, PBT II, PBT III and PBT IV on Fe (110) surface was carried out in order to locate the low energy adsorption sites of the potential corrosion inhibitors on Fe surface. Details of the methodology of Monte Carlo simulations are available in our previous publication [24].

3. Results and discussions

Outcomes of the weight loss experiment are presented in Table 2 and Fig. S1a (supplementary information). The protection abilities of PBTs are increasing with increasing their concentration and maximum value was obtained at $42.8 \times 10^{-5} \text{M}$ concentration. However, increase in the PBTs concentration from 34.2×10^{-5} to $42.8 \times 10^{-5} \text{M}$ did not causes significant improvement in their performance therefore in the present study former concentration is treated as optimum concentration. Inhibition efficiencies of PBTs follow the order: PBT-IV (94.886%) > PBT-III (92.613%) > PBT-II (90.340%) > PBT-I (86.931%). The order of protection ability can be described on the basis of PBTs molecular structure and nature of substituents present in their molecular structures. The value of Hammett substituent constants can be used to describe the order of inhibition efficiencies derived for PBTs. A substituent with negative value of Hammett

substituent constant (σ) is considered to be electron donor that can increase the electron density at donor sites and therefore facilitates the adsorption behavior of corrosion inhibitor [26, 27]. The values of σ for $-H$, $-CH_3$, $-OH$ and $-OCH_3$ substituents are 0.00, -0.17, -0.37 and -0.22, respectively. The inhibition efficiencies order of PBT-I, PBT-II and PBT-III can be explained on the basis of σ values of their substituent. Highest protection ability of the PBT-IV is attributed to the cumulative electron donating nature of its both $-OH$ and $-OCH_3$ substituents. Besides the substituents, increase in the molecular size on moving from PBT-I to PBT-IV because of the increase in the number and size of substituent(s) can also result in the increase of their inhibition performance.

Effect of temperature on the protection power of PBTs is shown in Table 3 and Fig. S1b. It can be seen that protection power of PBTs is decreasing on increasing electrolyte temperature. Acid catalyzed change in the molecular conformations, molecular rearrangement and molecular fragmentation at high temperature can be some possible factors for decrease in the protection ability of PBTs. More so, elevation in electrolyte temperature results into the kinetic energy of the PBT molecules which in turn decreases the attraction force between them and metallic surface. The Arrhenius equation can be used to express the effect of temperature on protection ability of PBTs [24, 25]:

$$\log(C_R) = \frac{-E_a}{2.303RT} + \log A \quad (10)$$

In Arrhenius equation all symbols have their usual meaning. A is the Arrhenius pre-exponential factor and E_a is the activation energy for corrosion process taking place with and without PBTs. The E_a values were (derived from the Arrhenius plots Fig. 2) 67.26 kJmol^{-1} , 74.62 kJmol^{-1} , 69.53 kJmol^{-1} and 72.60 kJmol^{-1} for PBT-I, PBT-II, PBT-III and PBT-IV, respectively. The E_a values for corrosion of mild steel in the presence of PBTs are extremely high as compared to in their absence that suggests that the process of corrosion in the presence of PBTs is highly difficult as compared to in their absence [28]. This observation leads to an idea that PBTs adsorb on the metallic surface and inhibit metallic dissolution.

Adsorption isotherm study for interaction of metal surfaces and electrolyte is one of the most interesting topics in corrosion inhibition. The outcomes of adsorption isotherm study give structural information about the electric double layer created over the metallic surface along with thermodynamic information. The surface coverage values obtained from weight loss experiments were fitted with the log of concentration in order to find the best adsorption isotherm. In the present study Langmuir, Temkin and Freundlich adsorption isotherms were fitted for PBTs

adsorption at the interfaces and presented in Fig. 3. Descriptors of the isotherms are presented in Table S1 (supplementary information) which show that adsorption of the PBTs on interface mainly follows the Temkin and Freundlich adsorption isotherms as the values of regression coefficient is most close to one in their cases. The tested isotherms can be presented as follows [29]:

$$K_{ads} C_{inh(M)} = \frac{\theta}{1-\theta} \quad (\text{Langmuir adsorption isotherm}) \quad (11)$$

$$K_{ads} C_{inh(M)} = \theta \quad (\text{Freundlich adsorption isotherm}) \quad (12)$$

$$K_{ads} C_{inh(M)} = \frac{\exp(a\theta) - 1}{1 - \exp[-a(1-\theta)]} \quad (\text{Temkin adsorption isotherm}) \quad (13)$$

In above equations, K_{ads} is the adsorption constant, $C_{inh(M)}$ is the molar concentration of PBTs, θ is the surface coverage and a is the molecular interaction factor. The degree metal-PBTs interactions can be derived in the term of K_{ads} . Obviously, a high magnitude of the K_{ads} is consisted with the high ability of adsorption and vice versa. In our present study, values of K_{ads} are lying in the range of 10^4 which imply that PBT molecules strongly interact with the metallic surface. Using the credential of the adsorption constant (K_{ads}), the values of standard Gibb's free energies (ΔG_{ads}^0) for the adsorption of PBT molecules were calculated using following relationship [24, 25]:

$$\Delta G_{ads}^0 = -RT \ln(55.5 K_{ads}) \quad (14)$$

In equation (14), numerical digit of 55.5 represents the aqueous concentration in acidic medium and other symbols have their usual meaning. Calculated values of ΔG_{ads}^0 for the adsorption of PBT molecules at different temperatures have been presented in Table 3. It is noticeable that value of ΔG_{ads}^0 either -40 kJmol^{-1} or more negative is associated with electrons (charge) sharing between inhibitor and metallic surface i.e. chemisorption while its value either -20 kJmol^{-1} or less negative is consistent with electrostatic interactions between charged metallic surface and inhibitor molecules. In strong acidic medium (like 1M HCl), rapid discharge of electrons (through oxidation) in to the electrolyte makes the metallic surface positively charged that attracts the inversely charged counter ions like chloride ions of HCl, sulfate ions of the H_2SO_4 , phosphate ions of H_3PO_4 , nitrate ions of HNO_3 etc. through electrostatic interactions. In other words, in electrolytic solutions metallic surface becomes negatively charged because of the

accumulation of counter ions. On the other hands, heteroatoms (N, O, S etc.) of the organic inhibitors easily undergo protonation and exist in cationic (protonated form). These two oppositively charged species fascinate each other through electrostatic force of attraction (physisorption mechanism). However, ones the inhibitor (PBT) molecules electrostatically adsorb over the metallic surface, the protonated heteroatoms uptake electrons from the metallic surface and revert in their neural forms with free unshared electron pairs. The heteroatoms transfer their unshared electrons pairs into the d-orbitals of the surface metallic atoms and form coordinate bonding (chemisorption). On the basis it is concluded that in most the metal-inhibitor (PBTs) interactions involve physiochemisorption mechanism (mixed type). For the adsorption of PBT molecules undertaken in the present study, values of ΔG_{ads}^0 are lying in the range of -31.0 kJmol⁻¹ to -35.6 kJmol⁻¹ which suggests that adsorption mechanism of PBT molecules is not purely physical or purely chemical but is of mixed type [24, 25].

Electrochemical behavior of PBT molecules on the mild steel acidic corrosion was carried out using open circuit potential (OCP), potentiodynamic polarization and electrochemical impedance spectroscopy (EIS) measurements. Potential generated on the metal-electrolyte interfaces deprived of applying any exterior potential is entitled as OCP. The OCP versus time curves for mild steel dissolution in 1M HCl with and without PBT molecules are shown in Fig. 4 (after 30 minutes immersion time). It can be seen that OCP versus time curves in all conditions represent straight lines which suggest that OCPs have been established after 30 minutes immersion time. It is important to mention that nonlinearity of the OCP versus time curve is mostly resulted due to the presence of surface oxide layers (Fe₂O₄ and Fe₃O₄) which slowly undergo dissolution after immersing the specimens into the corrosive electrolyte. Therefore, formation straight OCP versus time curves after 30 minutes immersion time indicate that oxide layers have been completely dissolved from the surface [30, 31]. More so, careful inspection shows that as compared to the black specimen, the inhibited OCP versus time curves have shifted slightly towards negative direction without affecting the common characteristics of OCP versus time curves. This finding suggests that PBT molecules mainly affect the cathodic reactions and behaved as cathodic type of inhibitors.

Potentiodynamic polarization (anodic and cathodic Tafel) curves for mild steel corrosive dissolution in 1M HCl with and without PBT molecules are presented in Fig. 5 and several parameters derived through extrapolation of the linear segments of the Tafel curves along with percentage of inhibition efficiency are presented in Table 4. It can be seen that the shape Tafel curves are similar in both inhibited and uninhibited cases which implies that PBT molecules do

not affect the mechanism of the mild steel corrosive dissolution. Results showed that values of corrosion current densities for inhibited (by PBTs) cases are very less as compared to the uninhibited case. This finding suggests that PBT molecules inhibit corrosion by adsorbing on the interfaces of the metal and electrolyte (1M HCl) [14, 32]. Adsorption of the PBT molecules results into the blockage of active sites responsible for the corrosive dissolution [14, 32]. Generally, an inhibitor can be classified into anodic or cathodic type depending upon the shift in the E_{corr} value of inhibited Tafel curves as compared to the E_{corr} value of uninhibited Tafel curve. If the shift is more than -85 mV then inhibitor may be of anodic or cathodic type and if the shift is less than -85 mV then inhibitor can be classified as mixed type. In our present study maximum shift in the E_{corr} values were 78 mV, 38 mV, 65 mV and 34 mV for PBT-I, PBT-II, PBT-III and PBT-IV, respectively which implies that PBT molecules are mixed type corrosion inhibitors [33]. However, results presented in the Table 4 showed that with respect to the anodic and cathodic Tafel slope values of blank, cathodic Tafel slope values show greater variation as compared to the value of anodic Tafel slopes. On the basis of above observations it can be predicted that though PBT molecule have less than -85 mV shift in the E_{corr} value but they can be categorized into cathodic type of inhibitors [34].

Nyquist and Bode plots for mild steel dissolution with and without PBT molecules are presented in Figs. 6a and 6b. Fitted Nyquist and Bode plots for mild steel corrosion in acidic medium of 1M HCl is shown in our previous report [35]. The Nyquist plots in both conditions show the single semicircle which implies that mild steel corrosion involves the single charge transfer mechanism which is also confirmed from the single maxima in the Bode plots [35]. It can be seen that diameter of the semicircle for inhibited (by PBT molecules) Nyquist plots are much higher as compared to the diameter of the Nyquist plot of blank specimen. Increased diameter of the inhibited Nyquist curves suggest that mild steel corrosion (charge transfer) from metal to electrolyte solution has become difficult in the presence of PBT molecules due to their adsorption at the metal-electrolyte interfaces [36]. It can also be seen that in the absence and presence of PBT molecules the shape of Nyquist plots are similar suggesting that PBT molecules do not affect the mechanism of corrosive dissolution. The EIS data were analyzed using an appropriate equivalent circuit reported in our earlier published reports [24, 25]. The circuit consists of three elements namely, solution resistance denoted by R_s , charge transfer resistance denoted by R_{ct} and constant phase element (CPE). The values of EIS parameters along with percentage of inhibition efficiencies for PBT molecules are presented in Table 4. It can be seen from the results that values of R_{ct} are much higher for inhibited cases as compared to the uninhibited case. This finding suggests that charge transfer from metal to electrolyte has become

significantly difficult due to the formation of protective inhibitive film at the metal-electrolyte interfaces. Following equation can be used to represents the impedance of CPE [24, 25]:

$$Z_{CPE} = Y_0^{-1} (i\omega)^{-1} \quad (15)$$

In the above equation, -1 represents an imaginary number, n is an exponent of CPE, Y is the CPE constant and ω is the angular frequency in rad s^{-1} . Generally, value of n is used as a gauss for surface inhomogeneity and behavior of CPE. A high value of n is associated with lower surface roughness and vice versa. On the basis of n value CPE can be defined as capacitor ($n=1$, $Y_0=C$), resistor ($n=0$, $Y_0=R$), inductance ($n=-1$, $Y_0=L$) or Warburg impedance ($n=1/2$, $Y_0=W$). In the present study values of n is almost equal to the unity for inhibited and uninhibited cases which implies that in the present case CPE behave as pseudo-capacitor [24, 25]. Deviation from the ideal capacitive behavior of the CPE is mostly attributed to the surface inhomogeneity resulted due to structural and interfacial origin. Following equation was employed to derive the values of C_{dl} (double layer capacitance) [24, 25]:

$$C_{dl} = (Y_0 R_{ct}^{1-n})^{1/n} \quad (16)$$

Results presented in Table 4 show that values of C_{dl} are much lower in the presence of PBT molecules as compared to in their absence and the values of R_{ct} just follow the inverse order. The decreased values of C_{dl} and increased values of R_{ct} in the presence of the PBT molecules is attributed to the adsorption of PBT molecules at metal-electrolyte (1M HCl) interfaces. The adsorbed PBT molecules form a protective barrier for corrosion process [37].

In order to support the trend of corrosion inhibition efficiencies of PBT molecules obtained by electrochemical and weight loss studies, the surface morphological examination of the inhibited and uninhibited metallic surfaces were carried out using SEM and AFM methods. The SEM and AFM images of the specimens are shown in Fig. 7 and 8, respectively. It can be seen that after 3 hrs immersion time surface of mild steel is highly corroded in the absence of PBT molecules. The surface of the uninhibited metallic specimen has been badly damaged showing several pits and cracks like appearance. However, in the presence of PBT molecules the SEM surface morphologies became relatively smoother. This finding suggests that PBT molecules form a surface protective covering which isolates the metals from aggressive acidic medium (1M HCl) and protect from corrosion. Similar observation is derived from the AFM analysis. The AFM image of uninhibited metallic surface shows some mountain like appearance that resulted due to corrosive damage of the surface in the absence of PBT molecules. However, in the presence of

PBT molecules the surface morphologies became smoother owing to their protection ability. The average surface roughness was 392 nm in the absence of PBTs where as in the presence of PBT-I, PBT-II, PBT-III and PBT-IV average surface roughness values were 218, 186, 172 and 154 nm, respectively. Decrease in the surface roughness values in the presence of PBTs suggested their adsorption and formation of protective film over the metallic surface.

In order to support the outcomes of weight loss, electrochemical and surface studies, density functional based quantum chemical calculations were performed on the investigated PBT molecules. Results of the DFT study are presented in Table 5 and frontier molecular orbitals of the neutral as well as protonated forms of PBT molecules are shown in Figs. 9 and 10. It is clearly perceptible that HOMO and LUMO electron distributions are mainly localized over the pyrimidobenzothiazole moiety for PBT-I, PBT-II and PBT-III suggesting that the pyrimidobenzothiazole moiety mostly involves in electron sharing that is metal-inhibitor bonding. However, in the case of PBT-IV, HOMO and LUMO are slightly also localized over the hydroxyl and methoxy substituted phenyl ring which suggests that the substituted phenyl ring is also involved in electron sharing that offers better metal-inhibitor interaction and high inhibition efficiency of PBT-IV as compared to the other PBT molecules. All investigated PBT molecules have several heteroatoms including nitrogen, oxygen and sulfur which can easily protonate in strong acidic solution of 1M HCl. Therefore, DFT study was also carried out on the protonated form of PBT molecules. The highest negative Mullikan charge containing heteroatom was selected as site for protonation. The Mullikan charges of the all atoms of PBT molecules are shown in Table S2 (supplementary information). The frontier molecular electron distribution of protonated PBT molecules is similar to their neutral form. However, the extent of HOMO and LUMO distribution for protonated form is relatively greater as compared to the neutral form of PBT molecules. Higher value of E_{HOMO} is associate with high electron donating ability of the molecule as compared to the molecule having lesser value of E_{HOMO} [24, 25]. Similarly, a lower value of E_{LUMO} is associated with high electron accepting tendency of the molecule from appropriate donor molecule as compared to the molecule having higher value of E_{LUMO} . Results showed that values of E_{HOMO} for both forms of PBT molecules are increasing on going from PBT-I to PBT-IV which implies that electron donating ability of the PBT molecules is increasing in the same sequence. Both neutral as well as protonated forms of PBT molecules showed the same and predictable trend of E_{HOMO} values. Though the values of E_{LUMO} did not show any regular trend however, lowest value of E_{LUMO} for PBT-IV (protonated) suggests that it has maximum electron accepting ability among the investigated PBT molecules and therefore it offers the maximum inhibition efficiency [38]. Conceivably, energy band gap (ΔE) is the most

important DFT parameters in the term of which chemical reactivity of any species or inhibition efficiency of an inhibitor molecule can be explained. In general, an inhibitor molecule with high magnitude of ΔE is supposed to be less reactive and underprivileged corrosion inhibitor as compared to the inhibitor molecule with low value of ΔE . Results showed that values of ΔE for neutral form of the PBT molecules did not showed any regular trend however a decreasing order of ΔE is observed in their protonated form. This observation revealed that chemical reactivities of the PBT molecules thereby their inhibition efficiencies toward mild steel corrosion in increasing on going from PBT-I to PBT-IV [39, 40]. According to the Pearson's theory, negative of the E_{HOMO} is regarded as ionization energy (IE) is and its low value is associated with high chemical reactivity as well as electron donating ability. For neutral as well as protonated forms of PBT molecules undertaken in the present investigation IE obeyed the order: PBT-IV < PBT-III < PBT-II < PBT-I which is in appropriate consistent with the experimental order of their inhibition efficiencies. Using same principal, negative of E_{LUMO} can be consider as electron affinity (EA). Similar to the value of E_{LUMO} , EA values also did not showed any predicted trend. However, highest value of EA for PBT-IV suggests that it has maximum electron accepting ability out of investigated PBT molecules. Electronegativity (χ) is measure of electron attracting ability of the atoms or molecules (global electronegativity). Obviously, a molecule with high value of global electronegativity is considered to be less reactive and non-preferred corrosion inhibitor because of the lesser metal-inhibitor interactions as compared to the molecule having less value of global electronegativity. Inspection of the results showed that values of χ for neutral as well as protonated PBT molecules are decreasing ongoing PBT-I to PBT-IV and therefore electron sharing tendency and corrosion inhibition efficiency of the BPT molecules are increasing in the same sequence [39, 41]. Hardness (η) is another DFT based reactivity parameter which is being frequently utilized to describe the metal inhibitor interactions. High value of global hardness is associated with low chemical reactivity and vice versa. In present study, for protonated form of PBT molecules values of hardness are decreasing ongoing PBT-I to PBT-IV which implies that chemical reactivity and corrosion inhibition efficiency of the PBT molecules enhance in the same sequence. Reciprocal of the hardness is regarded as softness (softness (σ) = 1/hardness (η)). It can be seen that for protonated form of PBT molecules the values of softness and thereby their corrosion inhibition behavior is increasing on moving PBT-I to PBT-IV [39, 42]. Lastly, values of fraction of electron transfer (ΔN) for PBT molecules were calculated and results showed that the values of ΔN are increasing on moving from PBT-I to PBT-IV which is consistent with the order of their protection abilities [25, 39]. In present study values of dipole moment (μ) did not show any regular trend however the PBT-IV molecule in neutral as well as

protonated forms showed the maximum value of dipole moment which suggests out of tested PBT molecules, PBT-IV has maximum tendency of polarizability when it comes in the contact with metallic surface that results into maximum surface coverage and highest inhibition efficiency of it [25, 39]. On the basis of above discussion related to the DFT study it can be summarized that PBT molecules act as good corrosion inhibitors and there their inhibition efficiencies derived from the DFT study well support the experimental results. Results of protonated form of PBT molecules are relatively more consistent with experimental results as compared to the results of neutral form of PBT molecules.

Recently, computational simulations using molecular dynamics and Monte Carlo and methods have attracted significant attention in the field of metallic corrosion inhibition using organic compounds. The sum of energies associated with inhibitor molecule ($E_{\text{inhibitor}}$), deformation energy (E_{def}) and rigid adsorption energy (E_{rigid}) can be regarded as total energy (E_{total}). The most stable and lowest energy conformation (top view) of the PBT-I, PBT-II, PBT-III and PBT-IV molecules on Fe (110) surface is depicted in Fig. 11 and the values of MC parameters such as E_{ads} , E_{rigid} , E_{total} , E_{int} , E_{def} and $dE_{\text{ads}}/dN_{\text{inh}}$ are given Table 6. It is clear that PBT molecules are adsorbed by their nearly flat or horizontal orientations. This observation suggests that there are more than one adsorption centers present in each PBT molecules through which they are being adsorbed horizontally. In present study value of iron surface (Fe (110)) is taken as zero for the calculation of several types of energy related to the PBT molecules adsorption. Energy (kcal/mol) released when one mole of the relaxed PBT molecules are adsorbed on substrate (iron) surface is termed as adsorption energy (E_{ads}) [29, 43]. Whereas, energy released during the adsorption of un-relaxed molecules (before geometric optimization) on the metallic surface is called as rigid adsorption energy (E_{rigid}) [29, 43]. The energy released when one mole of adsorbed inhibitor molecules relaxed over the metallic surface is called as deformation energy (E_{def}) [29, 43]. Obviously, a high value of E_{ads} is consisted with strong adsorption tendency of the inhibitor molecule and vice versa. Results showed that values of E_{ads} for PBT-I, PBT-II, PBT-III and PBT-IV molecules are increasing on moving from PBT-I to PBT-IV which suggests that effectiveness order of these molecules towards adsorption on mild steel surface follows the same trend [43-45]. Furthermore, for all investigated PBT molecules the values of E_{ads} are negative which implies that these molecules have spontaneous tendency of the adsorption over the metallic surface. Reciprocal of the adsorption energy is regarded as interaction energy (E_{int}). The highest value of E_{int} for PBT-IV indicates that it has strongest ability to interact with the metallic surface while converse it true for PBT-I [44-46]. The trend of

protection abilities of PBT molecules derived from MC simulations studies provides good support to the experimental as well as DFT studies.

4. Conclusions

From the present study following conclusions were drawn from the study:

1. Results showed that presence of electron releasing substituents such as $-\text{CH}_3$, $-\text{OH}$ and $-\text{OH}+-\text{OCH}_3$ enhances the effectiveness of the inhibitor molecules.
2. Their effectiveness followed the order: PBT-IV ($-\text{OCH}_3+ -\text{OH}$; 94.31%) > PBT-III ($-\text{OH}$; 92.20%) > PBT-II ($-\text{CH}_3$; 90.34%) > PBT-I ($-\text{H}$; 86.36%).
3. The PBT molecules adsorb on the metal-electrolyte interfaces and inhibit metallic dissolution. Investigated PBT molecules acted as cathodic type inhibitors.
4. Adsorption of the PBT molecules followed the Langmuir adsorption isotherm model.
5. SEM and AFM analyses suggested that presence of PBT molecules in the corrosive media smoothened the surface morphology of the metallic specimens.
6. DFT study carried out for neutral as well as protonated forms of PBT molecules provide good insight about the metal-PBTs interactions as well as support the experimental order of inhibition efficiency.
7. Results derived from MC study showed that PBT molecules adsorb spontaneously on metallic surface by their flat or horizontal orientations through their one or more adsorption centers.

Acknowledgements

CV thankfully acknowledges the North-West University (Mafikeng Campus) South Africa for providing the research support funds under Postdoctoral Fellowship Scheme.

References

- [1] F. Witte, V. Kaese, H. Haferkamp, E. Switzer, A. Meyer-Lindenberg, C. Wirth, H.J.B. Windhagen, In vivo corrosion of four magnesium alloys and the associated bone response, *Biomaterials*, 26 (2005) 3557-3563.
- [2] B. Orisanmi, S.A. Afolalu, O.R. Adetunji, E.Y. Salawu, I.P. Okokpue, A.A. Abioye, O. Akinyemi, O.P.J.I.J.o.A.E. Abioye, Cost of corrosion of metallic products in Federal University of Agriculture, Abeokuta, *International Journal of Applied Engineering Research*, 12 (2017) 14141-14147.
- [3] B. Hou, X. Li, X. Ma, C. Du, D. Zhang, M. Zheng, W. Xu, D. Lu, F.J.n.M.D. Ma, The cost of corrosion in China, *Materials Degradation*, 1 (2017) 1-10.
- [4] C. Verma, E.E. Ebenso, M.J.J.o.M.L. Quraishi, Ionic liquids as green and sustainable corrosion inhibitors for metals and alloys: An overview, *Journal of Molecular Liquids*, 233 (2017) 403-414.
- [5] L.L. Shreir, Corrosion: Corrosion control, Newnes Volume 2 (2013) .
- [6] M.G. Fontana, Corrosion engineering, Tata McGraw-Hill Education 2005.
- [7] M.A. Amin, M.M.J.C.S. Ibrahim, Corrosion and corrosion control of mild steel in concentrated H₂SO₄ solutions by a newly synthesized glycine derivative, *Corrosion Science*, 53 (2011) 873-885.
- [8] P.B. Raja, M. Ismail, S. Ghoreishiamiri, J. Mirza, M.C. Ismail, S. Kakooei, A.A.J.C.E.C. Rahim, Reviews on corrosion inhibitors: a short view, *Chemical Engineering Communications*, 203 (2016) 1145-1156.
- [9] C. Verma, L. Olasunkanmi, E.E. Ebenso, M. A. Quraishi, Substituents effect on corrosion inhibition performance of organic compounds in aggressive ionic solutions: A review, *Journal of Molecular liquids*, 251 (2018) 100-118.
- [10] V.S. Sastri, Green corrosion inhibitors: theory and practice, John Wiley & Sons 2012.
- [11] V.S. Sastri, Corrosion inhibitors: principles and applications, 1998.
- [12] M. Goyal, S. Kumar, I. Bahadur, C. Verma, E.E.J.J.o.M.L. Ebenso, Organic corrosion inhibitors for industrial cleaning of ferrous and non-ferrous metals in acidic solutions: a review, *Journal of Molecular liquids*, 256 (2018) 565-573.
- [13] A.M. Al-Sabagh, N.M. Nasser, A.A. Farag, M.A. Migahed, A.M. Eissa, T.J.E.J.o.P. Mahmoud, Structure effect of some amine derivatives on corrosion inhibition efficiency for carbon steel in acidic media using electrochemical and quantum theory methods, *Egyptian Journal of Petroleum*, 22 (2013) 101-116.
- [14] E. Oguzie, Y. Li, F.J.J.o.c. Wang, i. science, Corrosion inhibition and adsorption behavior of methionine on mild steel in sulfuric acid and synergistic effect of iodide ion, *Journal of colloid and interface science*, 310 (2007) 90-98.

- [15] E. Ebenso, U. Ekpe, B. Ita, O. Offiong, U.J.M.c. Ibok, physics, Effect of molecular structure on the efficiency of amides and thiosemicarbazones used for corrosion inhibition of mild steel in hydrochloric acid, *Materials Chemistry and Physics*, 60 (1999) 79-90.
- [16] J.E. Leffler, E. Grunwald, Rates and equilibria of organic reactions: as treated by statistical, thermodynamic and extrathermodynamic methods, Courier Corporation 2013.
- [17] Papavinasam, S. Corrosion Inhibitors, In: R. W. Revie (Ed.), Uhlig's Corrosion Handbook, Wiley, New Jersey, pp. 1021-1032 (2011).
- [18] M.C. Pirrung, K.D.J.J.o.t.A.C.S. Sarma, Multicomponent reactions are accelerated in water, *Journal of the American Chemical Society*, 126 (2004) 444-445.
- [19] A. Domling, W. Wang, K.J.C.r. Wang, Chemistry and biology of multicomponent reactions, *Chemical reviews*, 112 (2012) 3083-3135.
- [20] D.J. Ramón, M.J.A.C.I.E. Yus, Asymmetric multicomponent reactions (AMCRs): the new frontier, *Angewandte Chemie International Edition*, 2005 - Wiley Online Library, 44 (2005) 1602-1634.
- [21] V.K. Thakur, M.K.J.A.S.C. Thakur, Engineering, Recent advances in graft copolymerization and applications of chitosan: A review, *ACS Sustainable Chem. Eng.*, 2 (2014) 2637-2652.
- [22] E.J.P.i.P.S. Guibal, Heterogeneous catalysis on chitosan-based materials: a review, *Progress in Polymer Science*, 30 (2005) 71-109.
- [23] P.K. Sahu, P.K. Sahu, S.K. Gupta, D.D.J.I. Agarwal, E.C. Research, Chitosan: An efficient, reusable, and biodegradable catalyst for green synthesis of heterocycles, *Industrial & Engineering Chemistry Research*, 53 (2014) 2085-2091.
- [24] C. Verma, L.O. Olasunkanmi, E.E. Ebenso, M.A. Quraishi, I.B.J.T.J.o.P.C.C. Obot, Adsorption behavior of glucosamine-based, pyrimidine-fused heterocycles as green corrosion inhibitors for mild steel: experimental and theoretical studies, *Journal of Physical Chemistry C*, 120 (2016) 11598-11611.
- [25] C. Verma, L.O. Olasunkanmi, T.W. Quadri, E.-S.M. Sherif, E.E.J.T.J.o.P.C.C. Ebenso, Gravimetric, electrochemical, surface morphology, DFT, and Monte Carlo simulation studies on three N-substituted 2-aminopyridine derivatives as corrosion inhibitors of mild steel in acidic medium, *Journal of Physical Chemistry C*, 122 (2018) 11870-11882.
- [26] E.A. Noor, A.H.J.M.C. Al-Moubaraki, Physics, Thermodynamic study of metal corrosion and inhibitor adsorption processes in mild steel/1-methyl-4 [4'(-X)-styryl pyridinium iodides/hydrochloric acid systems, *Materials Chemistry and Physics*, 110 (2008) 145-154.
- [27] M. Abdallah, H. Al-Tass, B.A. Jahdaly, A.J.J.o.M.L. Fouda, Inhibition properties and adsorption behavior of 5-arylazothiazole derivatives on 1018 carbon steel in 0.5 M H₂SO₄ solution, *Journal of Molecular liquids*, 216 (2016) 590-597.
- [28] E.E.J.C.s. Oguzie, Corrosion inhibition of aluminium in acidic and alkaline media by Sansevieria trifasciata extract, *Corrosion science*, 49 (2007) 1527-1539.
- [29] C. Verma, H. Lgaz, D. Verma, E.E. Ebenso, I. Bahadur, M.J.J.o.M.L. Quraishi, Molecular dynamics and Monte Carlo simulations as powerful tools for study of interfacial adsorption behavior of corrosion inhibitors in aqueous phase: a review, *Journal of Molecular Liquids* (2018).

- [30] M. Migahed, M. Abd-El-Raouf, A. Al-Sabagh, H.J.E.A. Abd-El-Bary, Effectiveness of some non ionic surfactants as corrosion inhibitors for carbon steel pipelines in oil fields, *Electrochimica Acta*, 50 (2005) 4683-4689.
- [31] K. Ansari, M. Quraishi, A.J.C.S. Singh, Schiff's base of pyridyl substituted triazoles as new and effective corrosion inhibitors for mild steel in hydrochloric acid solution, *Corrosion Science*, 79 (2014) 5-15.
- [32] G. TrabANELli, V. Carassiti, Mechanism and phenomenology of organic inhibitors, *Advances in Corrosion Science and Technology*, Springer1970, pp. 147-228.
- [33] H.H. Hassan, E. Abdelghani, M.A.J.E.A. Amin, Inhibition of mild steel corrosion in hydrochloric acid solution by triazole derivatives: Part I. Polarization and EIS studies, *Electrochimica Acta*, 52 (2007) 6359-6366.
- [34] M. Desai, M. Desai, C. Shah, S.J.C.s. Desai, Schiff bases as corrosion inhibitors for mild steel in hydrochloric acid solutions, *Corrosion science*, 26 (1986) 827-837.
- [35] C. Verma, M. A. Quraishi, H. Lgaz, L.O.Olasunkanmi, El-Sayed M.Sherif, R.Salghi, E. E.Ebenso, Adsorption and anticorrosion behaviour of mild steel treated with 2-((1H-indol-2-yl)thio)-6-amino-4-phenylpyridine-3,5-dicarbonitriles in a hydrochloric acid solution: Experimental and computational studies, *Journal of Molecular Liquids*, 283 (2019) 491-506.
- [36] R.J.C.S. Solmaz, Investigation of the inhibition effect of 5-((E)-4-phenylbuta-1, 3-dienylideneamino)-1, 3, 4-thiadiazole-2-thiol Schiff base on mild steel corrosion in hydrochloric acid, *Corrosion Science*, 52 (2010) 3321-3330.
- [37] S.T. Selvi, V. Raman, N.J.J.o.a.e. Rajendran, Corrosion inhibition of mild steel by benzotriazole derivatives in acidic medium, *Journal of applied electrochemistry*, 33 (2003) 1175-1182.
- [38] S.K. Saha, A. Hens, A. RoyChowdhury, A.K. Lohar, N. Murmu, P.J.C.C.T. Banerjee, Molecular dynamics and density functional theory study on corrosion inhibitory action of three substituted pyrazine derivatives on steel surface, *Canadian Chemical Transactions*, 2 (2014) 489-503.
- [39] I. Obot, D. Macdonald, Z.J.C.S. Gasem, Density functional theory (DFT) as a powerful tool for designing new organic corrosion inhibitors. Part 1: an overview, *Corrosion Science*, 99 (2015) 1-30.
- [40] K. Laarej, M. Bouachrine, S. Radi, S. Kertit, B.J.J.o.C. Hammouti, Quantum chemical studies on the inhibiting effect of bipyrazoles on steel corrosion in HCl, *Journal of Chemistry*, 7 (2010) 419-424.
- [41] A. Yurt, Ö.J.C.S. Aykın, Diphenolic Schiff bases as corrosion inhibitors for aluminium in 0.1 M HCl: potentiodynamic polarisation and EQCM investigations, *Corrosion Science*, 53 (2011) 3725-3732.
- [42] Archana Pandey, Chandrabhan Verma, B. Singh, Eno E. Ebenso, Synthesis, characterization and corrosion inhibition properties of benzamidee2-chloro-4-nitrobenzoic acid and anthranilic acid and 2-chloro-4-nitrobenzoic acid for mild steel corrosion in acidic medium, *Journal of Molecular Structure*, 1155 (2018) 110-122.
- [43] Z. Salarvand, M. Amirnasr, M. Talebian, K. Raeissi, S.J.C.S. Meghdadi, Enhanced corrosion resistance of mild steel in 1 M HCl solution by trace amount of 2-phenyl-benzothiazole derivatives: Experimental, quantum chemical calculations and molecular dynamics (MD) simulation studies, *Corrosion Science*, 114 (2017) 133-145.

- [44] S. Kaya, L. Guo, C. Kaya, B. Tüzün, I. Obot, R. Tourir, N.J.J.o.t.T.I.o.C.E. Islam, Quantum chemical and molecular dynamic simulation studies for the prediction of inhibition efficiencies of some piperidine derivatives on the corrosion of iron, *Journal of the Taiwan Institute of Chemical Engineers*, 65 (2016) 522-529.
- [45] K.J.E.A. Khaled, Experimental and atomistic simulation studies of corrosion inhibition of copper by a new benzotriazole derivative in acid medium, *Electrochimica Acta*, 54 (2009) 4345-4352.
- [46] A.Y. Musa, R.T. Jalgham, A.B.J.C.S. Mohamad, Molecular dynamic and quantum chemical calculations for phthalazine derivatives as corrosion inhibitors of mild steel in 1 M HCl, *Corrosion Science*, 56 (2012) 176-183.

Figure Captions

Fig. 1. Synthetic procedure for PBT molecules.

Fig. 2. Arrhenius plots for mild steel corrosion in the absence and presence of PBT-I, PBT-II, PBT-III and PBT-IV molecules.

Fig. 3. (a) Langmuir, (b) Temkin and (c) Freundlich adsorption isotherms for PBT-I, PBT-II, PBT-III and PBT-IV adsorption on metallic substrate.

Fig. 4. OCP versus time curves for metallic dissolution in acidic medium with and without PBT-I, PBT-II, PBT-III and PBT-IV molecules.

Fig. 5. Polarization curves for metallic dissolution in acidic medium with and without PBT-I, PBT-II, PBT-III and PBT-IV molecules.

Fig. 6. (a) Nyquist and (b) Bode plots for metallic dissolution in acidic medium with and without PBT-I, PBT-II, PBT-III and PBT-IV molecules.
(c). equivalent circuit used to evaluate EIS data.

Fig. 7. SEM micrographs of mild steel surface (a) in the absence of PBTs and presence of (b) PBT-I, (c) PBT-II, (d) PBT-III and (e) PBT-IV molecules.

Fig. 8. SEM micrographs of mild steel surface (a) in the absence of PBTs and presence of (b) PBT-I, (c) PBT-II, (d) PBT-III and (e) PBT-IV molecules.

Fig. 9. Frontier molecular orbital pictures of the neutral PBT molecules derived using B3LYP (Lee-Yang-Paar) functional and 6-311G basis set.

Fig. 10. Frontier molecular orbital pictures of the protonated PBT molecules derived using B3LYP (Lee-Yang-Paar) functional and 6-311G basis set.

Fig. 11. Top views of the most stable configurations for the adsorption of (a) PBT I, (b) PBT II (c) PBT III and (d) PBT IV on Fe (110) surface calculated using Monte Carlo simulations.

Table Captions

Table 1: Characterization and molecular informations about the investigated PBT molecules.

Table 2: Weight loss parameters derived for mild steel dissolution in 1M HCl in the absence and presence of PBT-I, PBT-II, PBT-III and PBT-IV molecules.

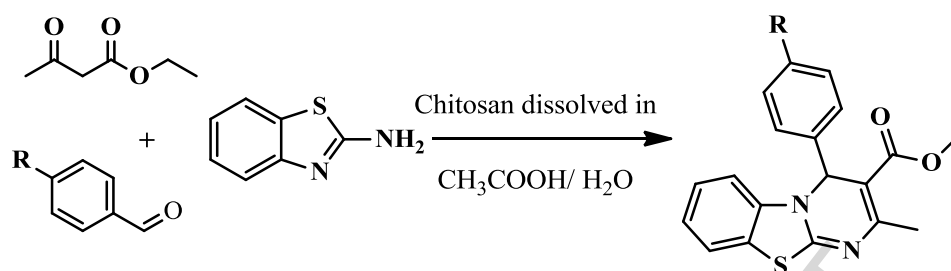
Table 3: Thermodynamic parameters derived through weight loss experiments at different temperatures (308-338K).

Table 4: PDP and EIS indices for mild steel corrosion in 1M HCl with and without PBT molecules.

Table 5: DFT parameters for neutral as well as protonated forms of PBT-I, PBT-II, PBT-III and PBT-IV molecules.

Table 6. The adsorption energies of PBT-I, PBT-II, PBT-III and PBT-IV on Fe (110) surface derived from Monte Carlo simulations (results in kcal/mol).

Figures



R= H, *p*-OMe, *p*-OH, *p*-OH-*m*-OMe

Fig. 1. Synthetic procedure for PBT molecules.

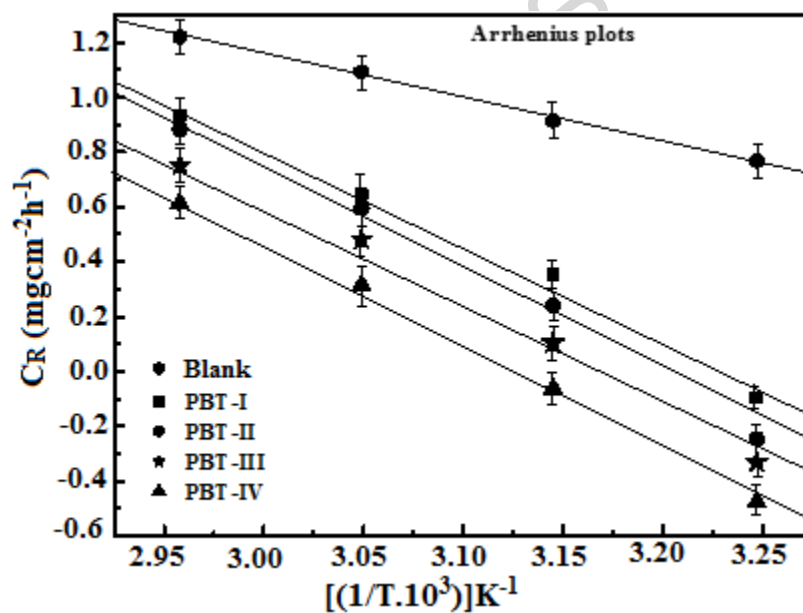
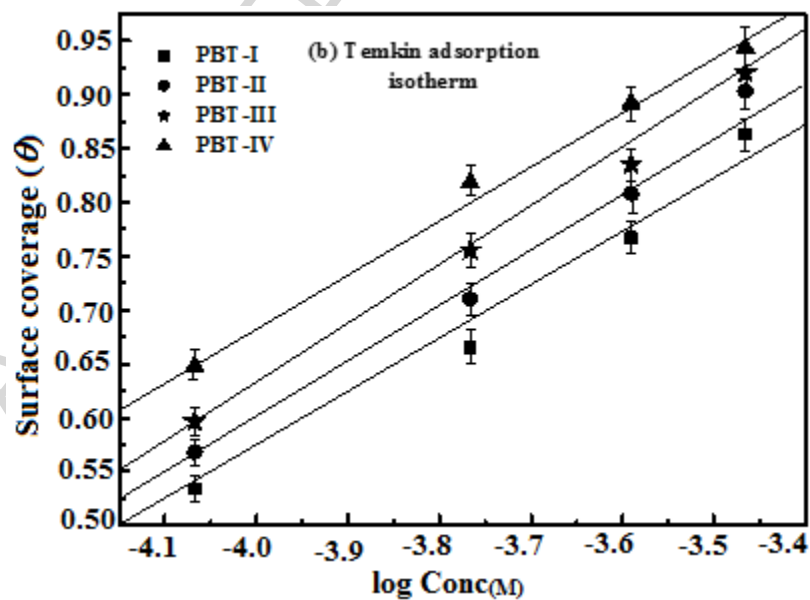
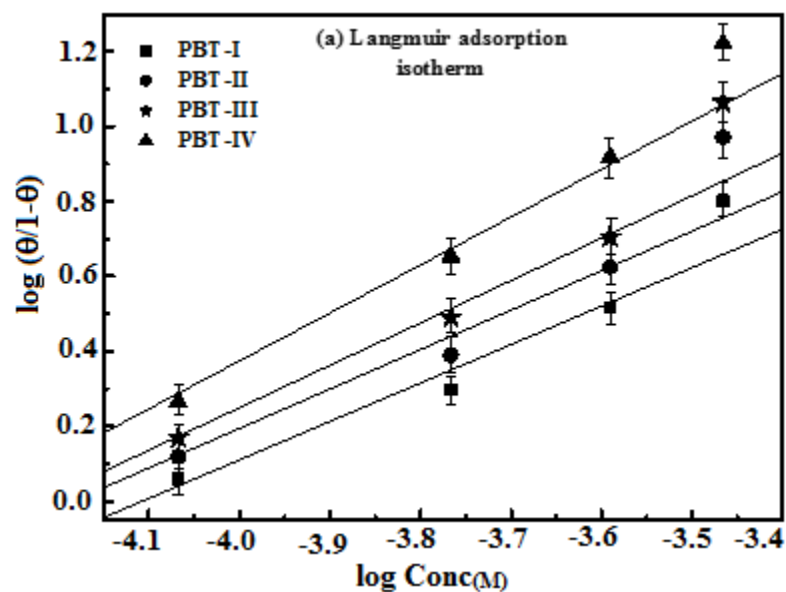


Fig. 2. Arrhenius plots for mild steel corrosion in the absence and presence of PBT-I, PBT-II, PBT-III and PBT-IV molecules.



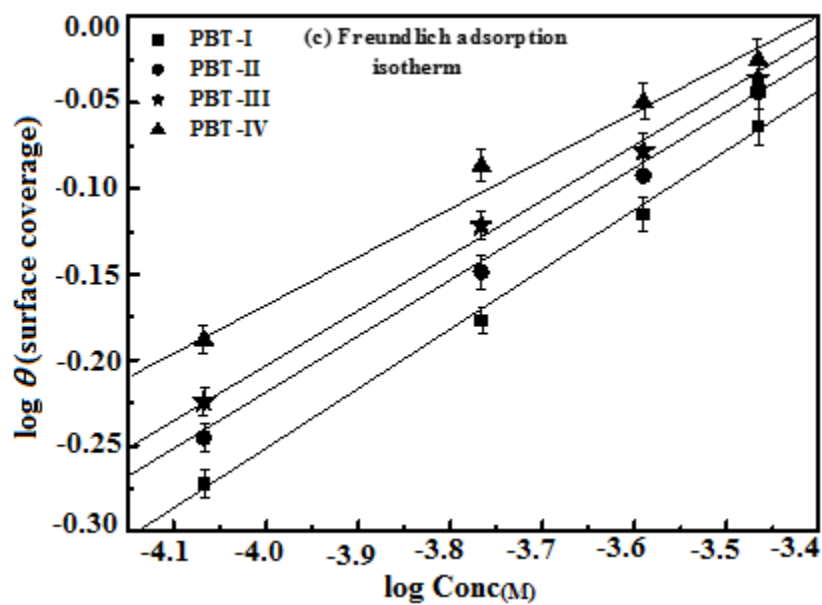


Fig. 3. (a) Langmuir, (b) Temkin and (c) Freundlich adsorption isotherms for PBT-I, PBT-II, PBT-III and PBT-IV adsorption on metallic substrate.

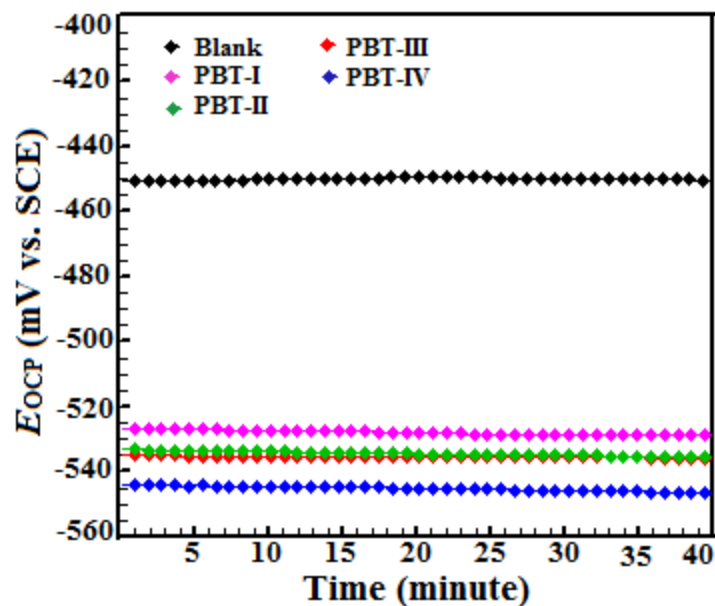


Fig. 4. OCP versus time curves for metallic dissolution in acidic medium with and without PBT-I, PBT-II, PBT-III and PBT-IV molecules.

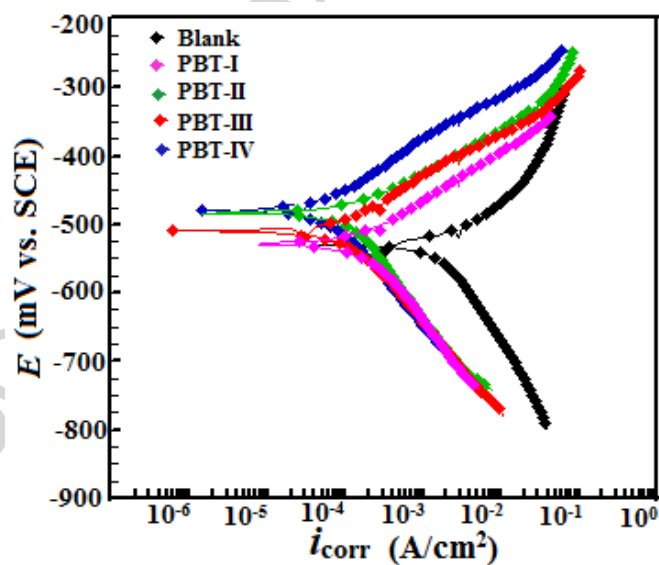


Fig. 5. Polarization curves for metallic dissolution in acidic medium with and without PBT-I, PBT-II, PBT-III and PBT-IV molecules.

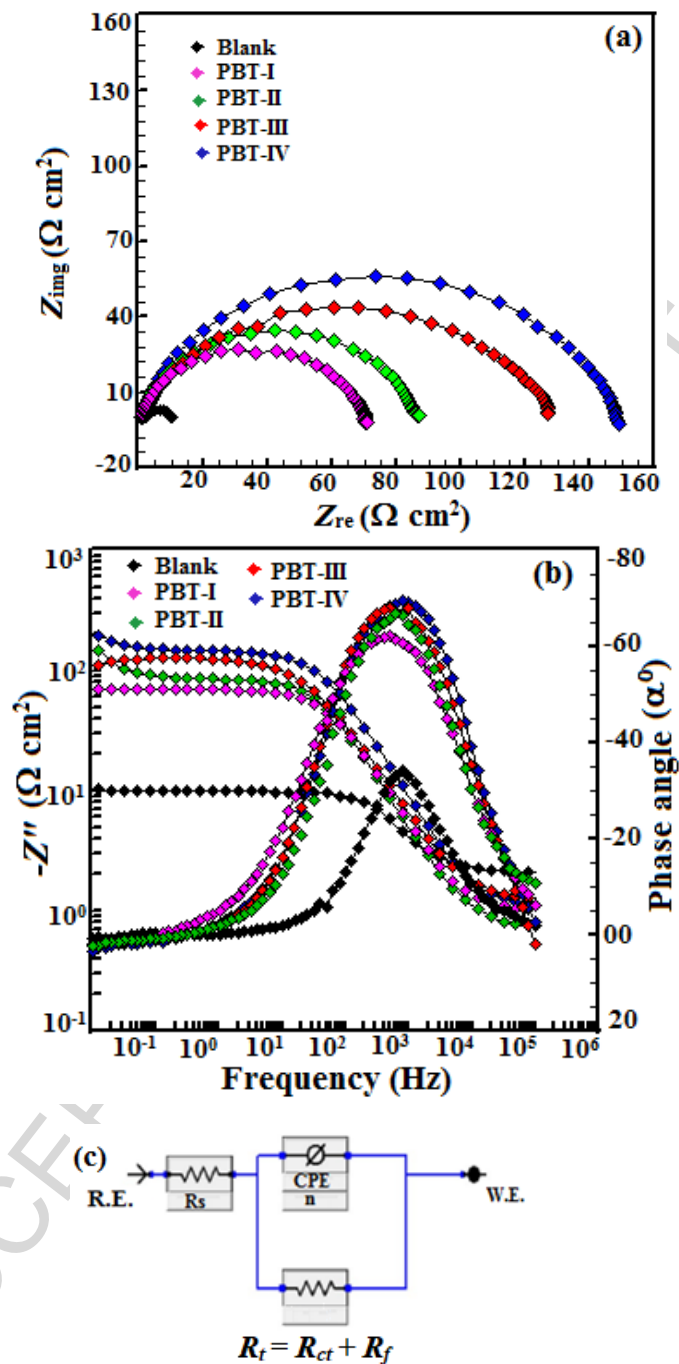


Fig. 6. (a) Nyquist and (b) Bode plots for metallic dissolution in acidic medium with and without PBT-I, PBT-II, PBT-III and PBT-IV molecules.
(c). equivalent circuit used to evaluate EIS data.

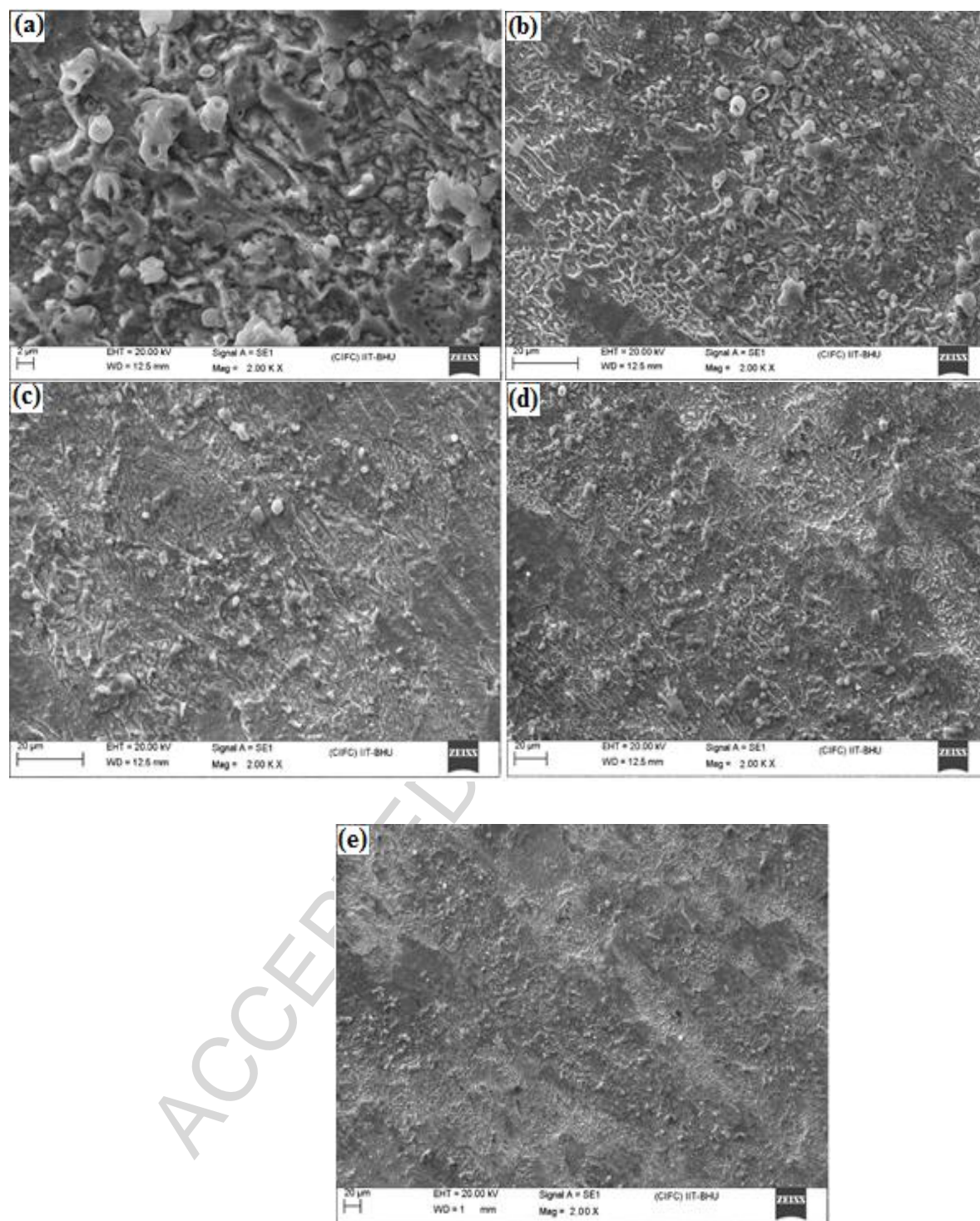


Fig. 7. SEM micrographs of mild steel surface (a) in the absence of PBTs and presence of (b) PBT-I, (c) PBT-II, (d) PBT-III and (e) PBT-IV molecules.

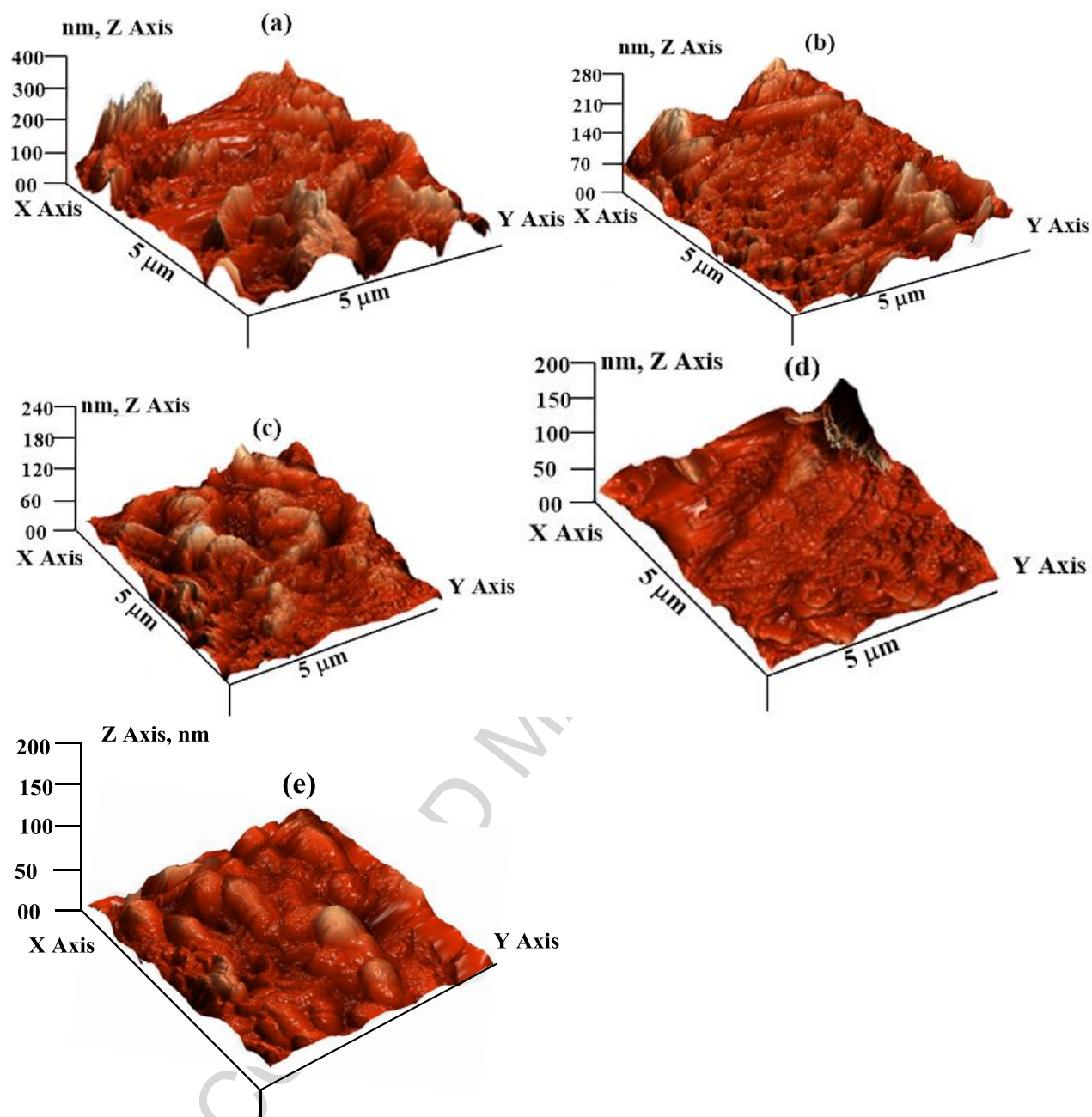


Fig. 8. SEM micrographs of mild steel surface (a) in the absence of PBTs and presence of (b) PBT-I, (c) PBT-II, (d) PBT-III and (e) PBT-IV molecules.

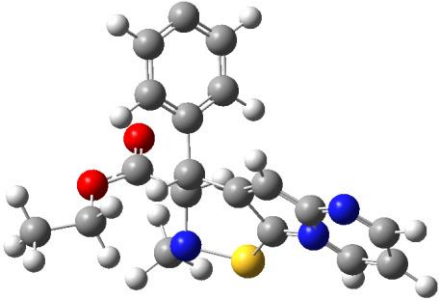
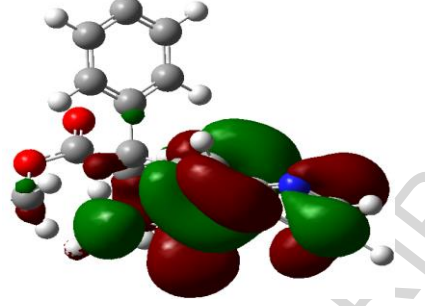
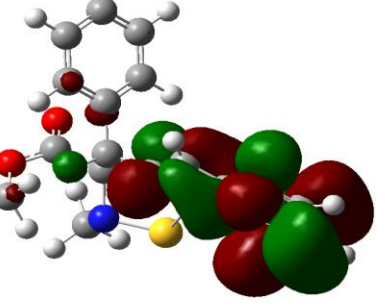
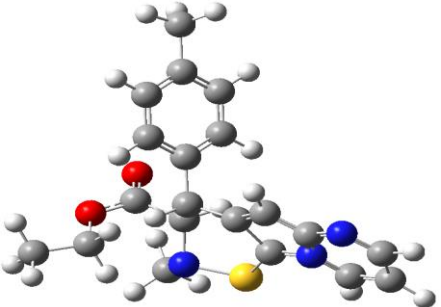
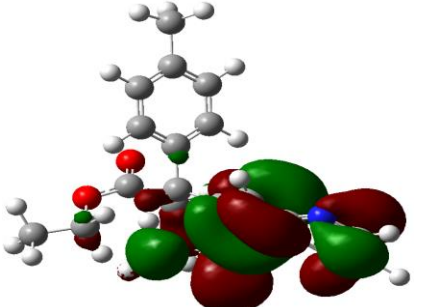
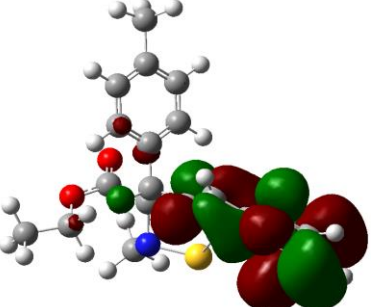
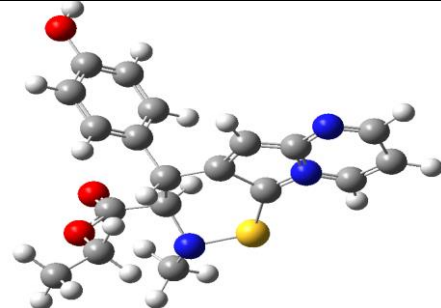
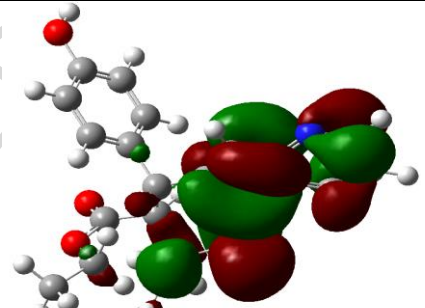
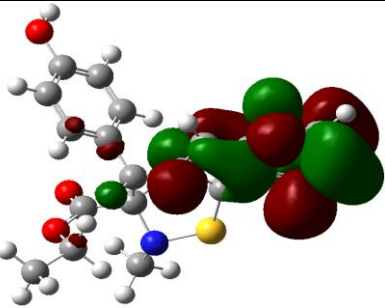
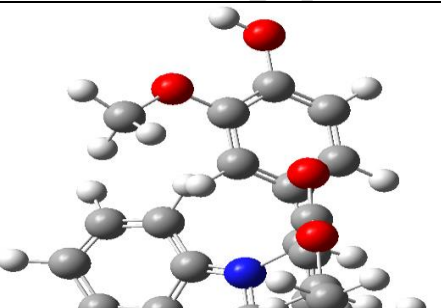
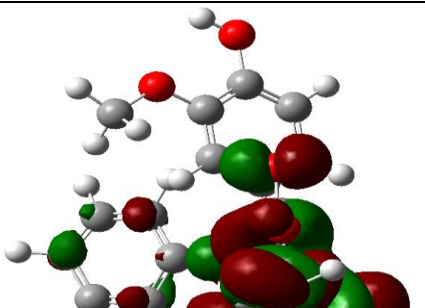
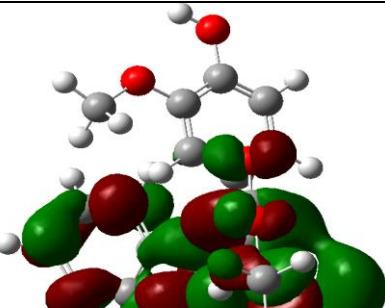
Inhibitor molecule	Frontier molecular orbital pictures		
	Optimized structure	HOMO	LUMO
PBT-I			
PBT-II			
PBT-III			
PBT-IV			

Fig. 9. Frontier molecular orbital pictures of the neutral PBT molecules derived using B3LYP (Lee-Yang-Paar) functional and 6-311G basis set.

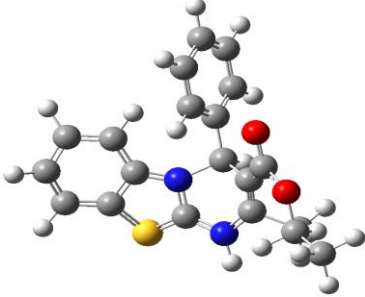
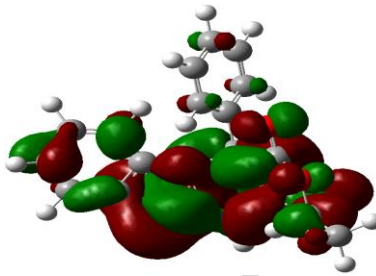
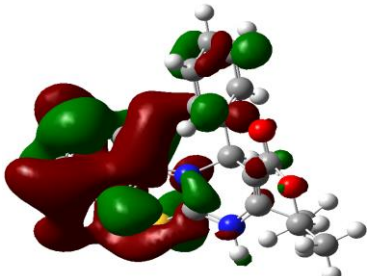
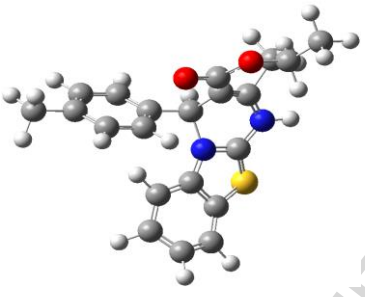
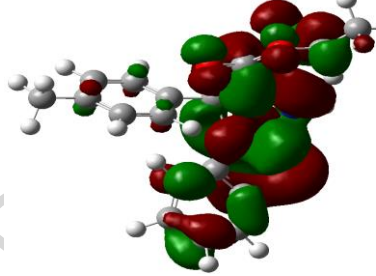
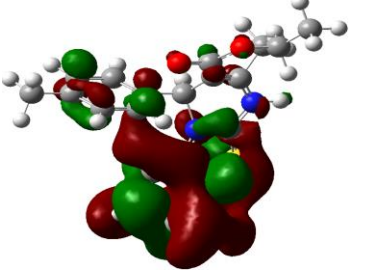
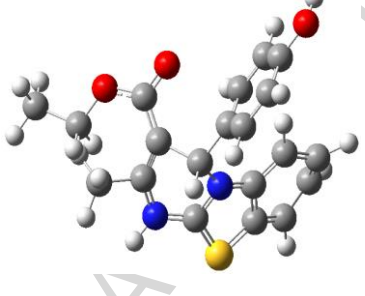
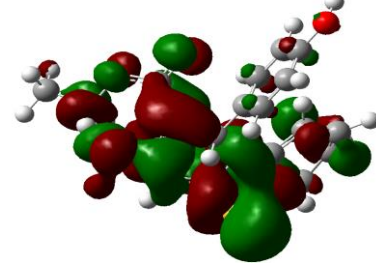
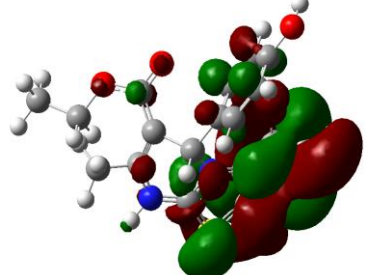
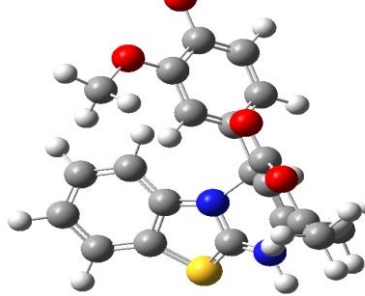
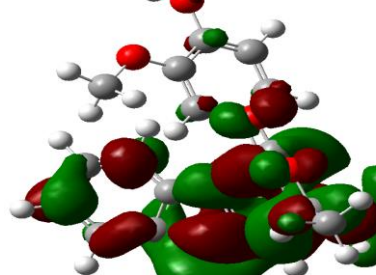
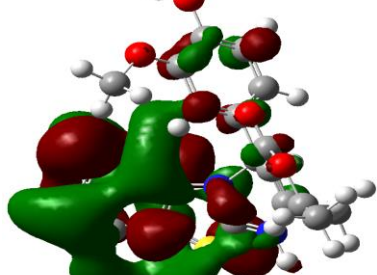
Inhibitor molecule	Frontier molecular orbital pictures		
	Optimized structure	HOMO	LUMO
PBT-IH ⁺			
PBT-IIH ⁺			
PBT-IIIH ⁺			
PBT-IVH ⁺			

Fig. 10. Frontier molecular orbital pictures of the protonated PBT molecules derived using B3LYP (Lee-Yang-Paar) functional and 6-311G basis set.

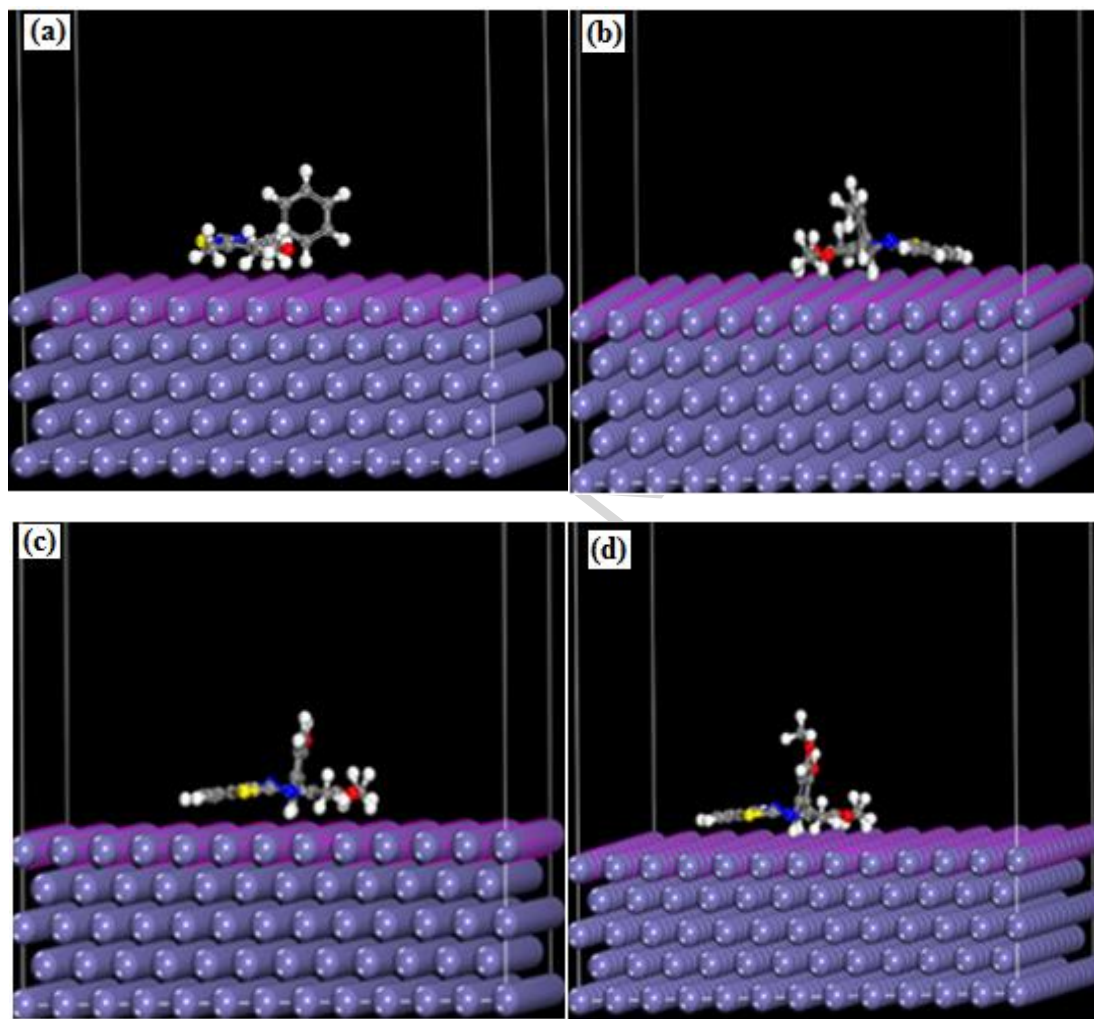


Fig. 11. Top views of the most stable configurations for the adsorption of (a) PBT I, (b) PBT II (c) PBT III and (d) PBT IV on Fe (110) surface calculated using Monte Carlo simulations.

Tables

Table 1: Characterization and molecular informations about the investigated PBT molecules.

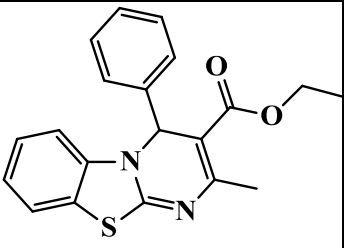
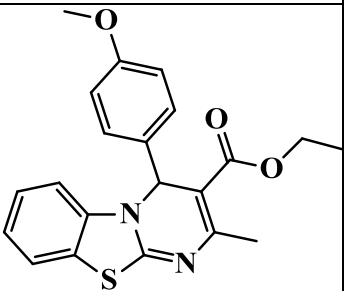
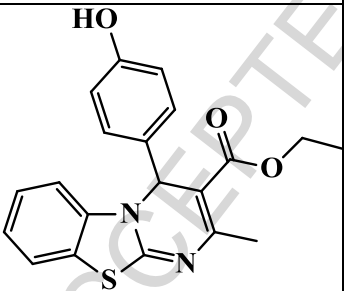
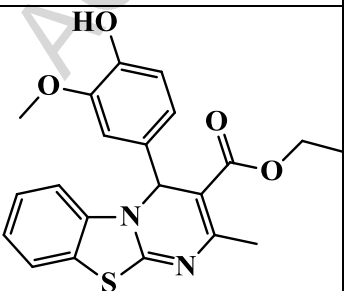
IUPAC name	Chemical structure	Analytical data
Ethyl 2-methyl-4-phenyl-4H-benzo[4,5]thiazolo[3,2-a]pyrimidine-3-carboxylate: ¹ (PBT-I); C ₂₀ H ₁₈ N ₂ O ₂ S		Yellow solid; yield = 68%; m.p. = 173-75 °C; FT IR (KBr) ν (cm ⁻¹): 3430, 3335, 1674, 1580, 1450, 1240; ¹ H NMR (500 MHz, CDCl ₃): 1.29 (t, 3H, -CH ₂ CH ₃), 2.45 (s, 3H, -CH ₃), 4.19 (q, 2H, -CH ₂ CH ₃), 6.42 (s, 1H), 7.10-7.45 (m, 9H, ArH); ¹³ C NMR (126 MHz, CDCl ₃): 166.21, 163.11, 141.05, 137.30, 128.34, 128.19, 127.02, 126.56, 124.03, 123.79, 122.07, 111.74, 103.01, 60.08, 57.73, 23.36, 14.21; E(m/z): 351 (M+1) ⁺ , 273 (100%). Elemental analysis: (Calc. for C ₂₀ H ₁₈ N ₂ O ₂ S: C, 68.55; H, 5.18; N, 7.99. Found: C, 66.87; H, 5.19; N, 7.97%).
Ethyl 4-(4-methoxyphenyl)-2-methyl-4H-benzo[4,5]thiazolo[3,2-a]pyrimidine-3-carboxylate: ¹ (PBT-II); C ₂₁ H ₂₀ N ₂ O ₃ S		Yellow solid; yield = 63%; m.p. = 141-43 °C; FT IR (KBr) ν (cm ⁻¹): 3420, 1705, 1509, 1243; ¹ H NMR (500 MHz, CDCl ₃): 1.25 (t, 3H, -CH ₂ CH ₃), 2.41 (s, 3H), 3.68 (s, 3H, ArOCH ₃), 4.08 (q, 2H, -CH ₂ CH ₃), 6.31 (s, 1H, -CH), 6.75-7.43 (m, 8H, ArH); ¹³ C NMR (126 MHz, CDCl ₃): 164.35, 159.96, 157.22, 151.98, 135.76, 131.48, 126.27, 124.39, 121.72, 121.63, 119.94, 111.67, 109.63, 101.04, 57.89, 55.04, 53.03, 21.32, 12.25. E (m/z): 381 (M+1) ⁺ . Elemental analysis: (Calc. for C ₂₁ H ₂₀ N ₂ O ₃ S: C, 66.29; H, 5.30; N, 7.36. Found: C, 66.31; H, 5.28; N, 7.35%).
Ethyl 4-(4-hydroxyphenyl)-2-methyl-4H-benzo[4,5]thiazolo[3,2-a]pyrimidine-3-carboxylate: ² (PBT-III); C ₂₀ H ₁₈ N ₂ O ₃ S		White solid; yield = 65%; m.p. = 172-74 °C; IR (KBr) ν (cm ⁻¹): 3360, 3077, 1713, 1689, 1462, 1230; ¹ H NMR (500 MHz, DMSO-d ₆): 1.20 (t, 3H, -CH ₂ CH ₃), 2.30 (s, 3H, -CH ₃), 4.01 (q, 2H, -CH ₂ CH ₃), 6.31 (s, 1H), 6.85-7.78 (m, 8H), 9.43 (s, 1H, -OH); ¹³ C NMR (126 MHz, DMSO-d ₆): 165.52, 162.24, 157.16, 153.49, 137.58, 132.11, 128.38, 122.76, 124.24, 122.75, 115.03, 112.29, 103.01, 59.33, 56.08, 23.11, 14.05; E (m/z): 367 (M+1) ⁺ . Elemental analysis: (Calc. for C ₂₀ H ₁₈ N ₂ O ₃ S: C, 65.55; H, 4.95; N, 7.64. Found: C, 65.41; H, 4.98; N, 7.63%).
Ethyl 4-(4-hydroxy-3-methoxyphenyl)-2-methyl-4H-benzo[4,5]thiazolo[3,2-a]pyrimidine-3-carboxylate: ² (PBT-IV); C ₂₁ H ₂₀ N ₂ O ₄ S		Yellow solid; yield = 58%; m.p. = 193-94 °C; FT IR (KBr) ν (cm ⁻¹): 3376, 3060, 2980, 1705, 1601, 1590, 1240; ¹ H NMR (500 MHz, CDCl ₃): 1.30 (t, 3H, -CH ₂ CH ₃), 2.45 (s, 3H, CH ₃), 3.86 (s, 3H, -OCH ₃), 4.15 (q, 2H, -CH ₂ CH ₃), 6.33 (s, 1H, -CH), 6.75-7.38 (m, 7H, ArH), 9.78 (s, 1H, -OH); ¹³ C NMR (126 MHz, CDCl ₃): 165.61, 162.36, 153.52, 147.14, 146.43, 137.61, 132.53, 126.39, 122.23, 115.19, 111.93, 110.90, 59.30, 55.44, 23.11, 14.09. E (m/z): 397 (M+1) ⁺ . Elemental analysis: (Calc. for C ₂₁ H ₂₀ N ₂ O ₄ S: C, 63.62; H, 5.08; N, 7.07. Found: C, 63.52; H, 5.13; N, 7.04%).

Table 2: Weight loss parameters derived for mild steel dissolution in 1M HCl in the absence and presence of PBT-I, PBT-II, PBT-III and PBT-IV molecules.

Inhibitor	Conc. (M)	Weight loss (mg)	C_R (mgcm ⁻² h ⁻¹)	$\eta\%$	θ
Blank	---	176 (± 1.414)	5.86(± 0.059)	---	---
PBT-I	8.56×10^{-5}	82(± 1.414)	2.733(± 0.047)	53.40	0.534
	17.1×10^{-5}	59(± 1.414)	1.966(± 0.047)	66.47	0.664
	25.7×10^{-5}	41(± 1.414)	1.366(± 0.047)	76.70	0.767
	34.2×10^{-5}	24(± 0.707)	0.800(± 0.023)	86.36	0.863
	42.8×10^{-5}	23(± 0.707)	0.766(± 0.023)	86.93	0.869
PBT-II	8.56×10^{-5}	76(± 1.414)	2.533(± 0.047)	56.81	0.568
	17.1×10^{-5}	51(± 1.414)	1.700(± 0.047)	71.02	0.710
	25.7×10^{-5}	35(± 0.707)	1.166(± 0.023)	80.81	0.808
	34.2×10^{-5}	17(± 0.707)	0.566(± 0.023)	90.34	0.903
	42.8×10^{-5}	17(± 0.707)	0.566(± 0.023)	90.34	0.903
PBT-III	8.56×10^{-5}	71(± 1.414)	2.366(± 0.047)	59.65	0.596
	17.1×10^{-5}	43(± 1.414)	1.433(± 0.047)	75.56	0.755
	25.7×10^{-5}	29(± 0.707)	0.966(± 0.023)	83.5	0.835
	34.2×10^{-5}	14(± 0.707)	0.466(± 0.023)	92.04	0.920
	42.8×10^{-5}	13(± 0.707)	0.433(± 0.023)	92.61	0.926
PBT-IV	8.56×10^{-5}	62(± 1.414)	2.066(± 0.047)	64.77	0.647
	17.1×10^{-5}	32(± 1.414)	1.066(± 0.047)	81.81	0.818
	25.7×10^{-5}	19(± 0.707)	0.633(± 0.023)	89.20	0.892
	34.2×10^{-5}	10(± 0.707)	0.333(± 0.023)	94.31	0.943
	42.8×10^{-5}	9(± 0.707)	0.300(± 0.023)	94.88	0.948

Table 3: Thermodynamic parameters derived through weight loss experiments at different temperatures (308-338K).

Temp	Blank		PBT-I				PBT-II				PBT-III				PBT-IV			
	C_R	$\eta\%$	C_R	$\eta\%$	K_{ads}	$-\Delta G^\circ$	C_R	$\eta\%$	K_{ads}	ΔG°	C_R	$\eta\%$	K_{ads}	$-\Delta G^\circ$	C_R	$\eta\%$	K_{ads}	$-\Delta G^\circ$
308	5.86	-	0.80	86.3	0.76	-33.2	0.56	90.3	1.12	-34.1	0.46	92.0	1.38	-34.7	0.33	94.3	1.99	-35.6
318	8.20	-	2.26	72.3	0.31	-31.9	1.73	78.8	0.44	-32.8	1.26	84.5	0.65	-33.8	0.86	89.4	1.01	-35.0
328	12.4	-	4.43	64.2	0.21	-31.8	3.93	68.2	0.25	-32.3	3.03	75.5	0.37	-33.3	2.06	83.3	0.60	-34.6
338	16.6	-	8.53	48.5	0.11	-31.0	7.63	54.0	0.14	-31.6	5.63	66.0	0.23	-33.0	4.10	75.3	0.36	-34.3

Table 4: PDP and EIS indices for mild steel corrosion in 1M HCl with and without PBT molecules.

		EIS parameters				Polarization parameters					
Inhibitors	R_s ($\Omega \text{ cm}^2$)	R_{ct} ($\Omega \text{ cm}^2$)	n	$\eta\%$	θ	E_{corr} (mV/SCE)	β_a (mV/dec)	$-\beta_c$ (mV/dec)	i_{corr} ($\mu\text{A}/\text{cm}^2$)	$\eta\%$	θ
Blank	1.120	9.58	0.827	---	---	-445.0	70.50	114.6	1150.0	---	---
PBT-I	1.002	68.96	0.868	86.10	0.86	-523.0	72.70	135.2	163.0	85.82	0.85
PBT-II	0.742	90.40	0.863	89.40	0.98	-483.0	64.80	200.0	129.0	88.78	0.88
PBT-III	1.217	122.6	0.844	92.18	0.92	-510.0	78.40	121.9	93.0	91.91	0.91
PBT-IV	1.111	150.9	0.867	93.65	0.93	-479.0	89.60	136.3	62.9	94.53	0.94

Table 5: DFT parameters for neutral as well as protonated forms of PBT-I, PBT-II, PBT-III and PBT-IV molecules.

Inhibitor	E _{HOMO} (eV)	E _{LUMO} (eV)	ΔE (eV)	IE (eV)	EA (eV)	χ (eV)	η (eV)	σ (eV)	ΔN (eV)	μ Debye
PBT-I	-4.985	-1.710	3.275	4.985	1.710	3.348	1.637	0.610	0.467	2.525
PBT-II	-4.810	-0.910	3.899	4.810	0.910	2.860	1.949	0.512	0.517	2.677
PBT-III	-4.270	-0.946	3.323	4.270	0.946	2.638	1.661	0.601	0.683	3.455
PBT-IV	-4.130	-1.134	2.996	4.130	1.134	2.632	1.498	0.667	0.749	4.940
PBT-IH ⁺	-4.465	-0.930	3.534	4.465	0.930	2.698	1.767	0.565	0.617	5.845
PBT-IIH ⁺	-4.425	-0.902	3.522	4.425	0.902	2.664	1.761	0.567	0.628	5.568
PBT-IIIH ⁺	-4.381	-0.910	3.471	4.381	0.910	2.645	1.735	0.576	0.643	5.900
PBT-IVH ⁺	-4.131	-0.961	3.169	4.131	0.961	2.546	1.584	0.631	0.736	7.231

Table 6. The adsorption energies of PBT-I, PBT-II, PBT-III and PBT-IV on Fe (110) surface derived from Monte Carlo simulations (results in kcal/mol).

Structures	E_{total}	E_{ads}	E_{rigid}	E_{def}	dE _{ad} /dNi	E_{binding}
Fe (1 1 0) – PBT I	-239.65	-174.26	-180.97	6.71	-174.26	174.26
Fe (1 1 0) – PBT II	-250.82	-177.29	-183.42	6.13	-177.29	177.29
Fe (1 1 0) – PBT III	-257.97	-177.31	-181.89	4.57	-177.31	177.31
Fe (1 1 0) – PBT IV	-243.56	-177.39	-182.77	5.38	-177.39	177.39

Highlights

1. Inhibition effect of four Pyrimido [2,1-B] Benzothiazoles (PBTs) was investigated.
2. Their efficiencies increase with their concentration.
3. PBTs act as cathodic type inhibitors.
4. MD simulations suggested that PBTs aligned horizontally (flatly) on the metallic surface.
5. Adsorption of the PBTs followed the Langmuir adsorption isotherm model.

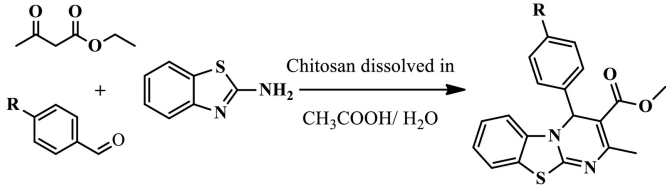


Figure 1

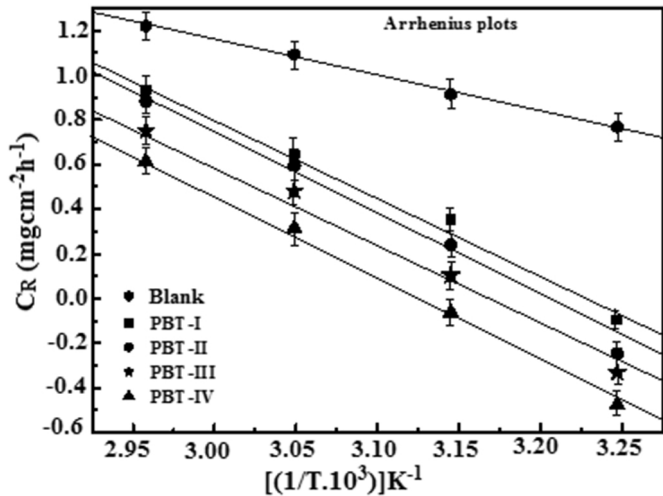


Figure 2

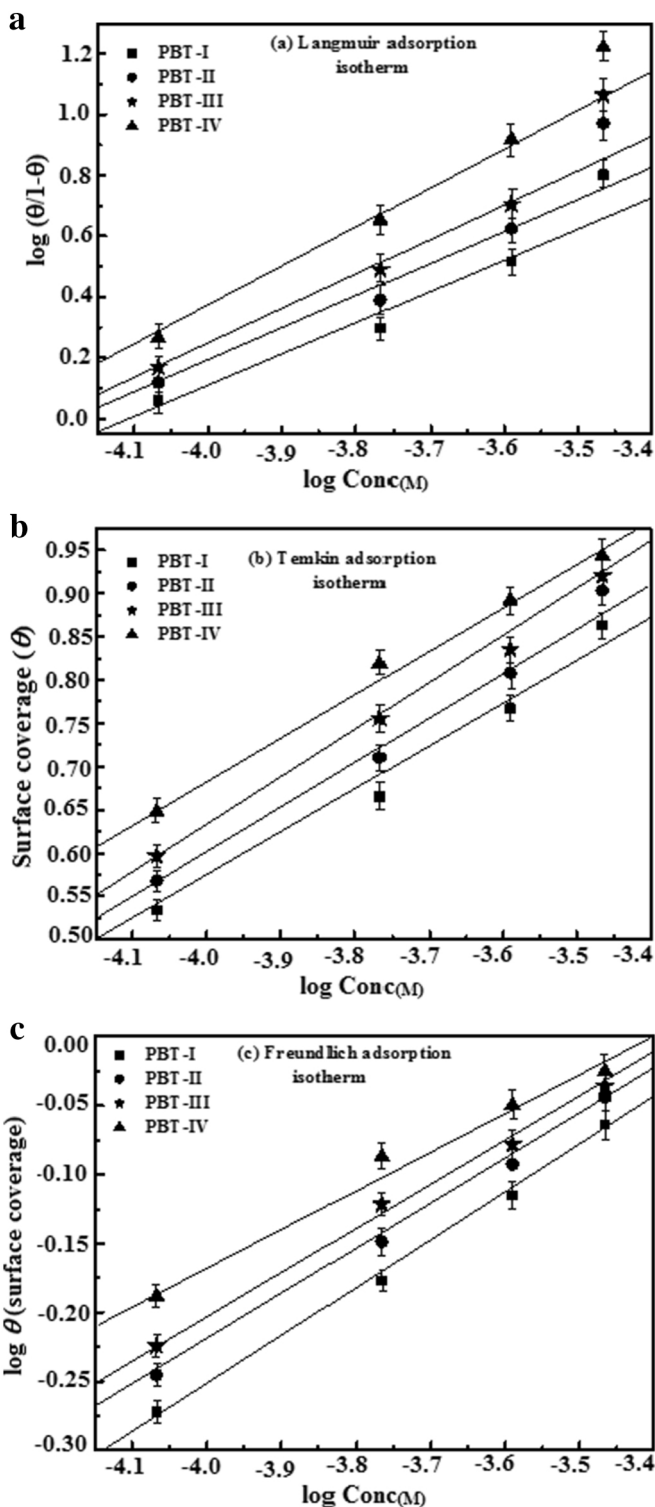


Figure 3

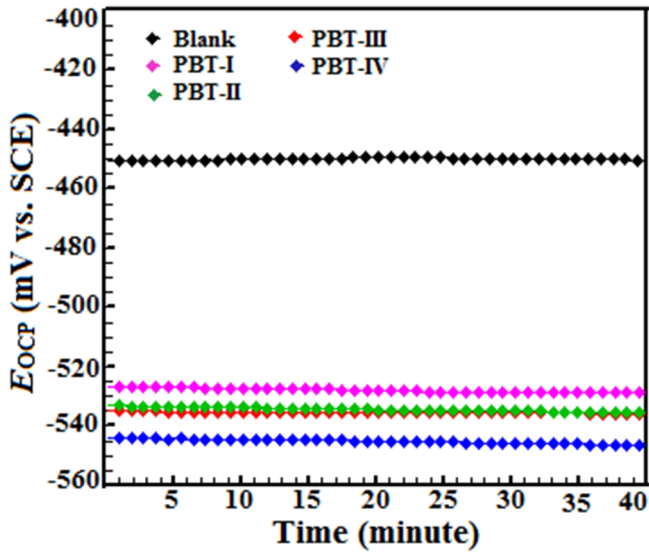


Figure 4

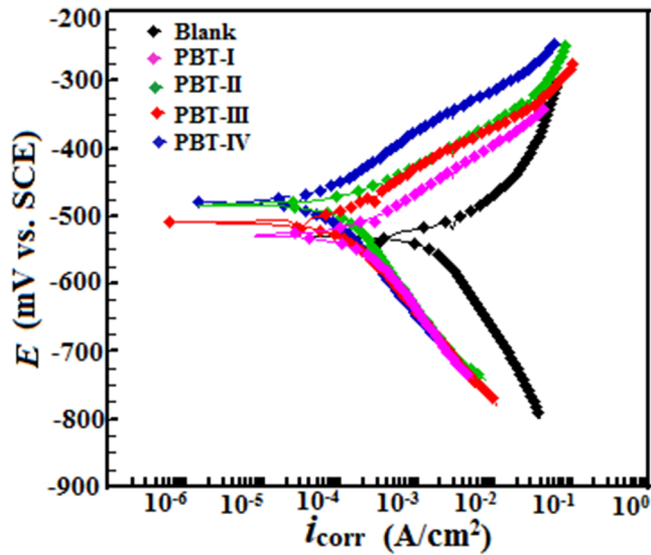


Figure 5

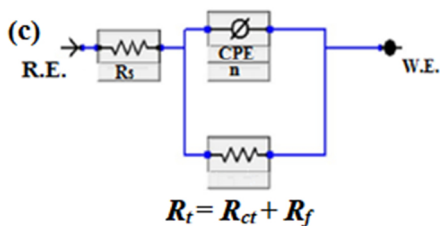
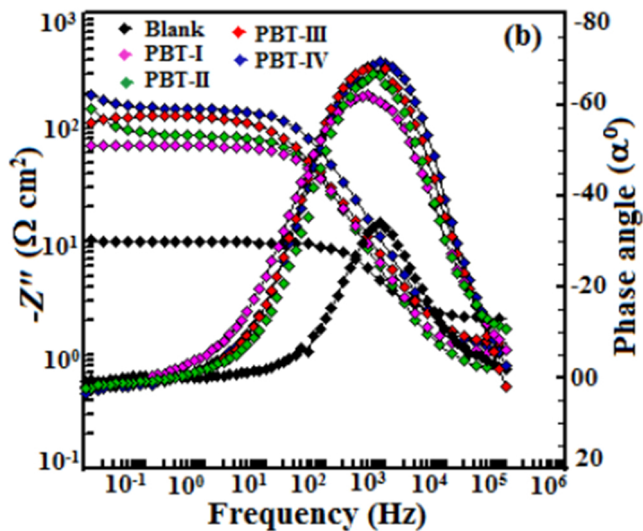
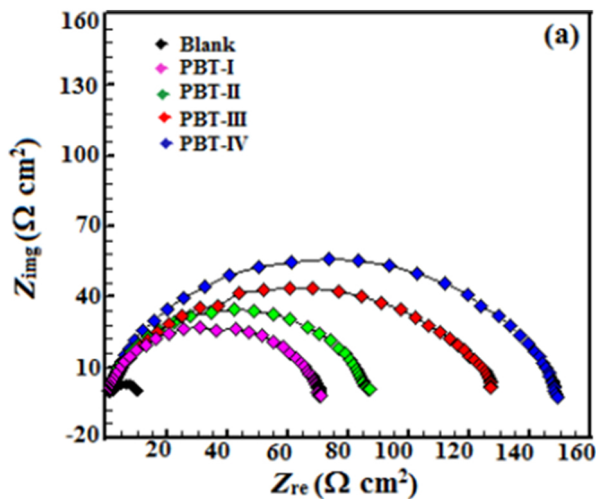


Figure 6

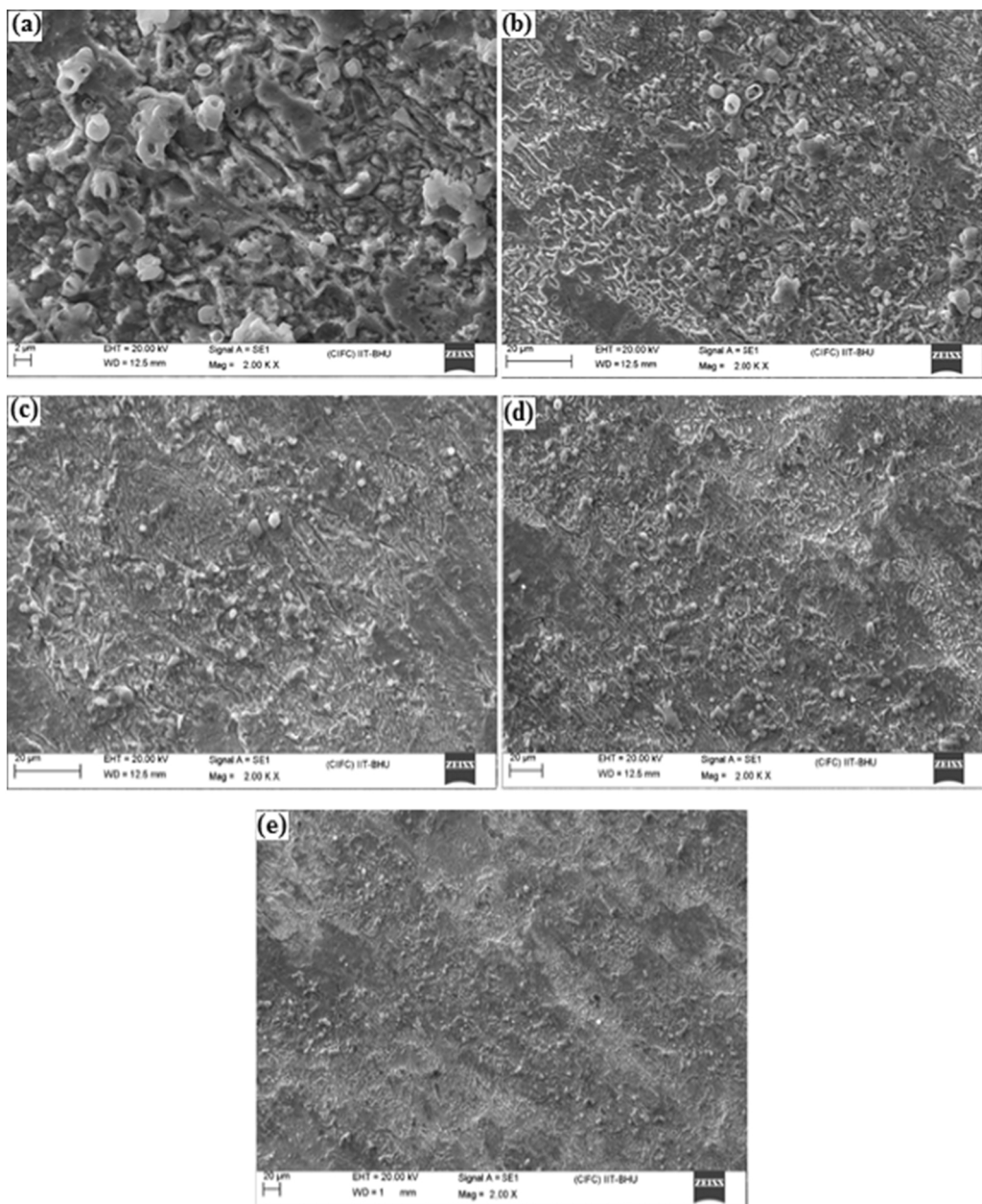


Figure 7

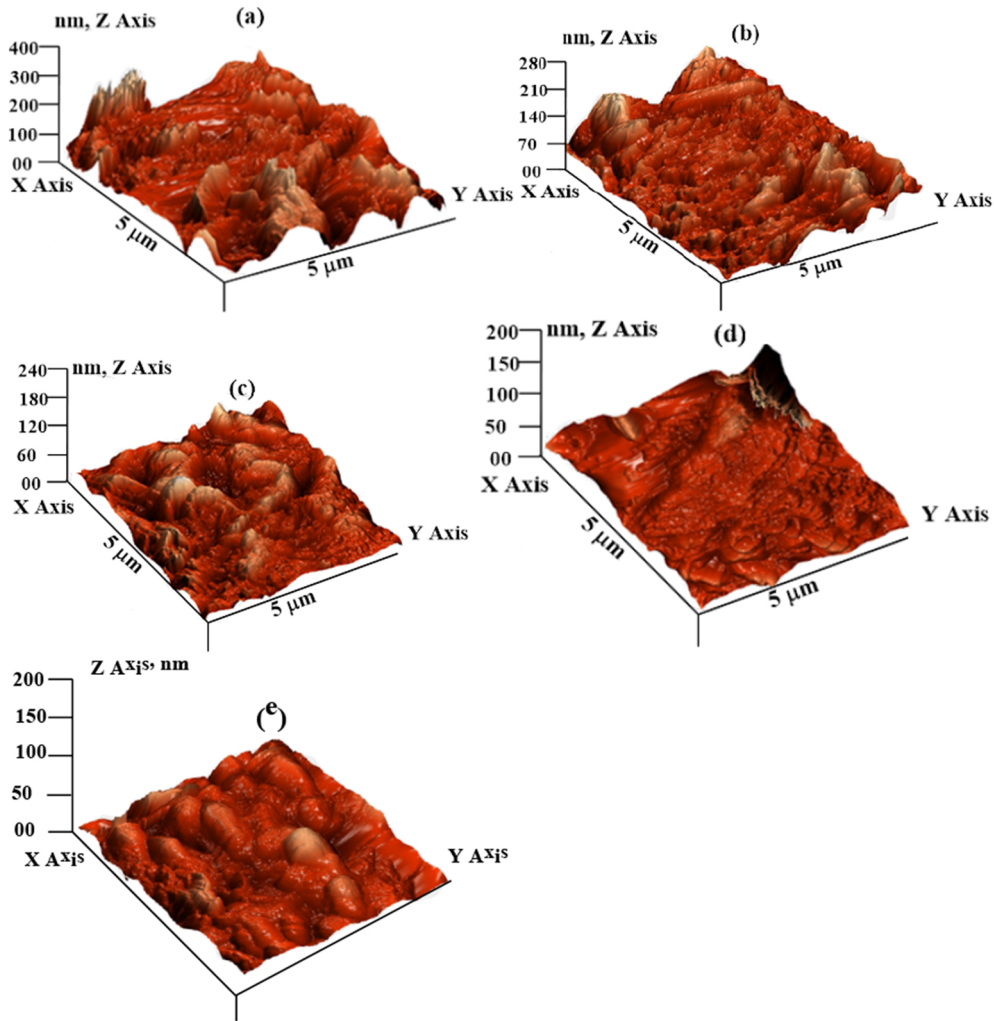


Figure 8

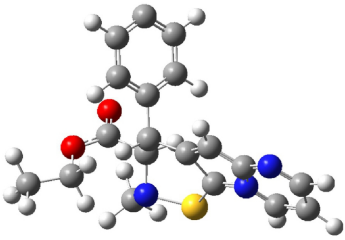
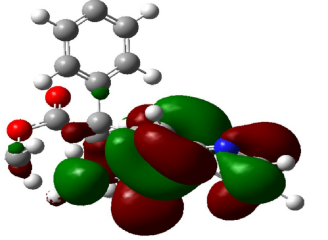
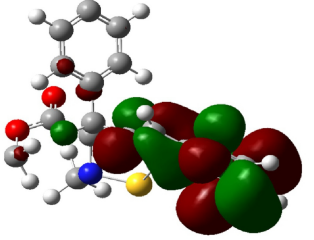
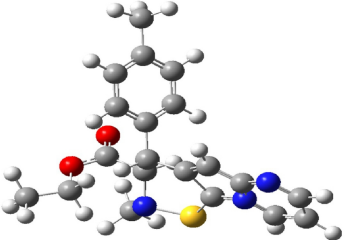
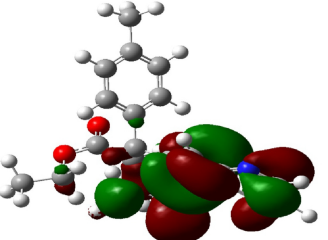
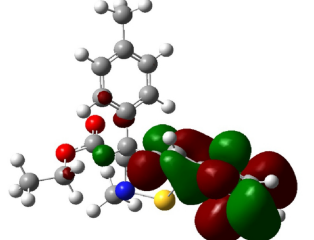
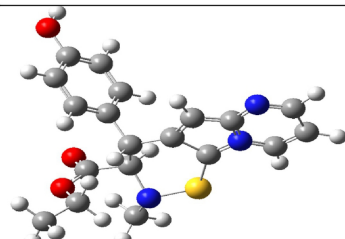
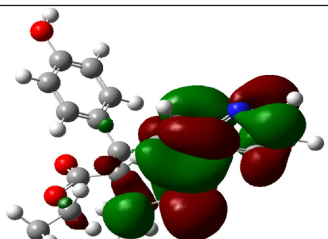
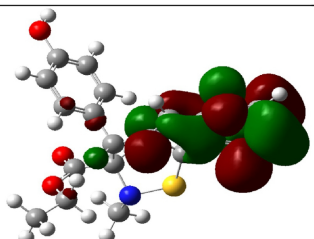
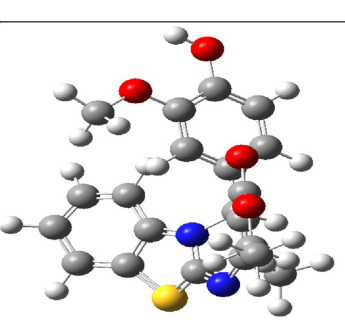
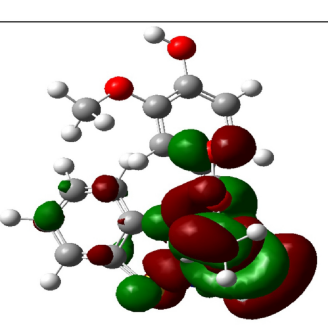
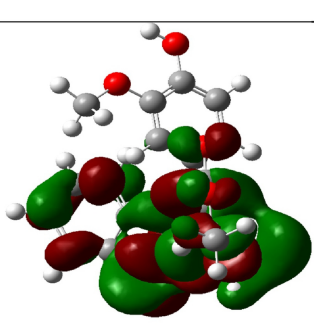
Inhibitor molecule	Frontier molecular orbital pictures		
	Optimized structure	HOMO	LUMO
PBT-I			
PBT-II			
PBT-III			
PBT-IV			

Figure 9

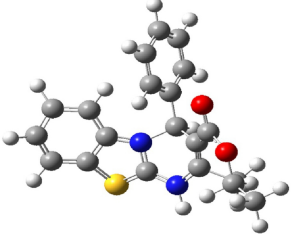
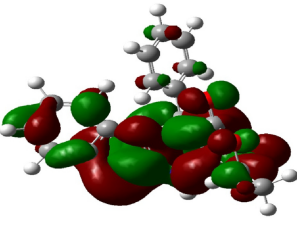
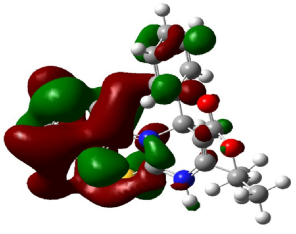
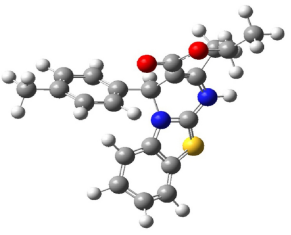
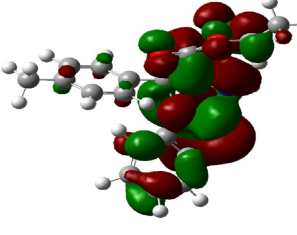
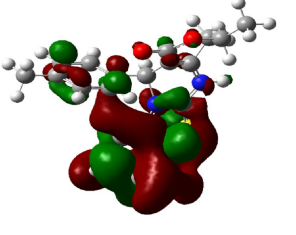
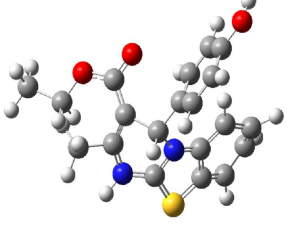
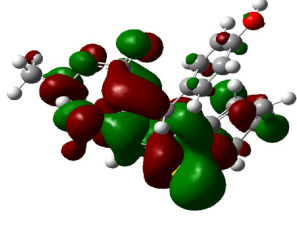
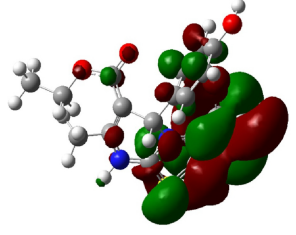
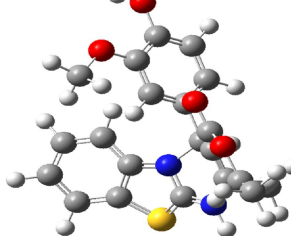
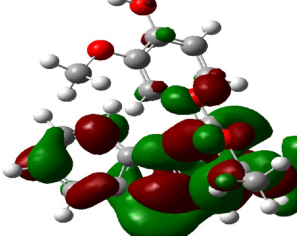
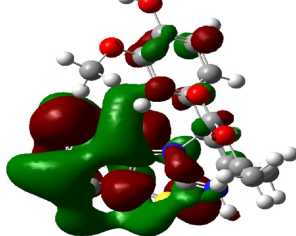
Inhibitor molecule	Frontier molecular orbital pictures		
	Optimized structure	HOMO	LUMO
PBT-IH ⁺			
PBT-IIH ⁺			
PBT-IIIH ⁺			
PBT-IVH ⁺			

Figure 10

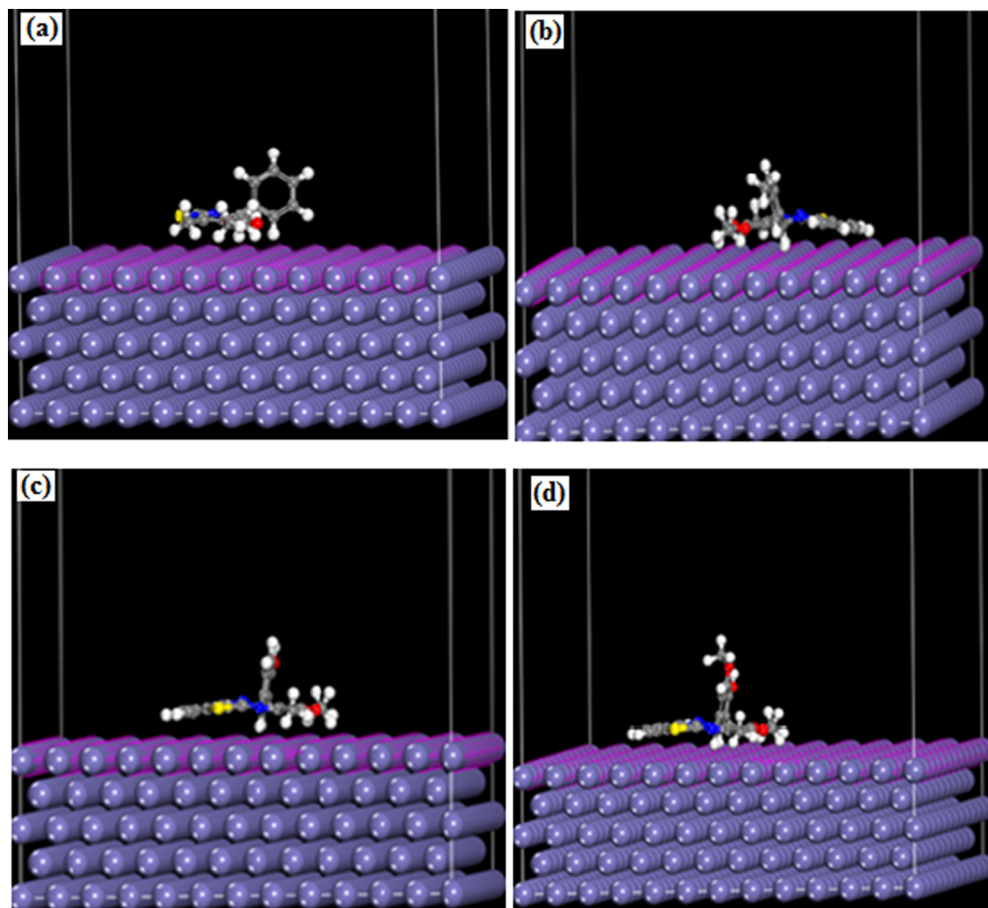


Figure 11